Understanding Bayesian stellar distance and stellar parameter estimation

Calin Jilavu

Lund Observatory
Lund University

2019-EXA151

Degree project of 15 higher education credits
June 2019

Supervisor: Paul McMillan

Lund Observatory
Box 43
SE-221 00 Lund
Sweden

Abstract

The consensus in the field is that we have a pretty good understanding of the physics behind star formation and evolution. So far, the models that have been created characterize the different collections of stars in our Milky Way galaxy with decent accuracy, and they have allowed for humanity to obtain insights into how our universe evolved. However, the author believes that our current techniques and theory that go into such models might be biased or slightly flawed.

A simulated model of the Milky Way is used to generate virtual stars whose properties are known. These stars are then analysed using the current most up-to-date techniques, and the obtained values for the various stellar properties are compared with the already known values. Non-trivial evidence is obtained that we are indeed systematically over-/underestimating the values of these parameters by almost 1 standard deviation in most cases. Some possible ideas about why this might be the case are explored within this document.

Populärvetenskaplig beskrivning

Astronomi är ett vetenskapsområde som får allt mer uppmärksamhet varje år, allteftersom vi blickar mot stjärnorna för framtida utforskning och kolonisation. Det är därför väldigt viktigt att mänskligheten fortsätter att arbeta med att förstå hur universum fungerar när det kommer till avlägsna stjärnor. Vi lär oss om detta genom att, bland annat, skapa modeller och simuleringar av vår galax baserade på vad vi vet från observationer och teorier. Det här hjälper oss att förbättra vår dataanalys.

Men, vi tror att våra nuvarande tekniker och teorier som krävs för att skapa sådana modeller för att analysera data kan vara vinklade eller bristfälliga. Det skulle vara väldigt problematiskt om det är så, och det är därför viktigt att ta ett steg tillbaka och reflektera över våra nuvarande metoder för att försäkra oss om att de är tillräckligt noggranna. I det här projektet kommer vi därför att testa de här teknikerna och kortfattat förklara de möjliga orsakerna till alla funna systematiska avvikelser.

Hur tänker vi testa våra tekniker?

Vi skapar en ”simulerad galax”, liknande vår egen Vintergata, med samlingar av virtuella stjärnor fördelade i galaxen enligt nuvarande teorier. Vi samlar sedan in data om de här stjärnorna, egenskaper som vanligtvis mäts i undersökningar (som temperatur, ytgravitation, hur mycket de lyser i olika delar av det elektromagnetiska spektrumet, etcetera). Sen analyserar vi varje stjärna med de senaste analysteknikerna för att beräkna vilka egenskaper som passar den bäst, baserat på de ursprungliga villkoren. Eftersom vi vet allting om de simulerade stjärnorna, kan vi jämföra deras egenskapers faktiska värden med de vi har beräknat. Skillnader mellan de observerade och beräknade värdena informerar oss om systematiska fel i de teknikerna som vi har använt. Vi upprepar processen för olika antaganden om fördelningen av stjärnor för att försäkra oss om att vi inte själva har introducerat ett systematiskt fel.

Det visar sig att de flesta huvudseriestjärnornas, stjärnor som Solen, massor blir underskattade, medan det motsatta stämmer för jättestjärnor. Mindre skillnader upptäcktes för ålder, ytgravitation och avstånd till stjärnorna, jättestjärnor var mest påverkade. Orsakerna till detta kan vara allt från systematiska fel i de mätningar som använts för att modellera stjärnorna till att börja med, till brister i denna studies metodologi. Trots det visar projektet på att det kan finnas djupare fel med våra nuvarande tekniker. Vidare studier krävs för att försäkra oss om att vi är på rätt spår i vår strävan efter kunskap om astronomi.

Contents

List of Figures

List of Tables

Chapter 1

Introduction

In order to achieve a better understanding of the Milky Way (and, in turn, other galaxies) we must first understand the basic building blocks that make it up, namely its stars. Thus, the accurate determination of stellar properties is of great importance for this endeavour. However, these properties are not necessarily easy to obtain.

One of the more common ways to determine stellar ages, structural parameters (e.g. effective temperature) and distances is to combine information from various surveys (astrometric, photometric or spectroscopic) into a Bayesian framework. This framework can then be used to determine stellar properties and, by extension, properties of the Milky Way. Therefore, it would be in our interest to perform tests on such a framework in order to determine its feasibility and perhaps gain some insights into our current theories and techniques.

1.1 Goal

The aim of this project is to investigate the results obtained from such a framework in order to determine if they are what we would expect or if they might be biased in some way. The project will make use of a piece of software named Galaxia (Sharma et al. 2011) used to create surveys of "fake stars" on which to test models and conduct investigations with another piece of software used in a previous study (McMillan et al. 2018), which applies the Bayesian approach.

The process of measuring distances to stars and objects in the far reaches of space is not as simple as it sounds. Since distances are enormous from star to star and even more so between galaxies, in terms of measurables we can obtain, we only have access to the light emitted by these objects. However, many other measurables can be derived just from spectral measurements, among which are effective temperatures, surface gravity of stars, and metallicities. Some of these parameters (such as the distance to a star) are harder to obtain and involve the use of multiple techniques and relations in parallel. For instance, parallaxes (e.g. from missions such as Gaia) can be used to determine distances (with better accuracy for closer stars). Likewise, photometry (i.e. colours of stars) can give a

good idea about effective temperatures.

Thus, it would be important to make sure that the theory and techniques used in astronomy provide accurate descriptions of these stellar parameters. In short, this project is not about presenting a new technique of obtaining data, rather its purpose is to make sure the current techniques are not flawed in some regard. The way this project intends to perform the tests is through the use of simulated models based on our current theory of stellar populations in galaxies.

A provisional answer to the question of expected results would be that, using our current knowledge of stellar parameter determination, we can successfully recreate realistic data with good accuracy from the aforementioned "fake surveys" of stars. This would suggest that our current methods for determining stellar properties can be trusted and applied with confidence to larger scale structures such as star clusters and galaxies. Subsequently, the research into the complex evolution of stellar populations within galaxies will have made another step forward with us successfully having been able to create "fake stellar populations" (albeit not fully simulated, but with most mechanisms involved in their evolutions modelled to an acceptable degree). This, of course, would also mean that all our current data on stellar parameters can be trusted, and that our instruments are not biased in any way.

Another possible outcome of the project could be that our simulated stellar populations yield unexpected data which might mean one of two things. The first explanation could be that the software used to model the stars is not detailed enough to offer an accurate enough of a simulation. The alternative case could be that the real measured data is biased in some way due to our instruments or our methods of interpreting it with our current theory.

1.2 Bayesian approach

In this project we apply Bayes' theorem when analysing data and determining the stellar parameters. The idea of the theorem is reasonably simple, and it is explored in more detail in Box & Tiao (2011). In essence: when creating a model, a prior distribution, which represents "what is known about unknown parameters" is used when introducing data. In stellar surveys for instance, we can use the information that low-mass stars are more common than high-mass stars as a prior distribution when analysing and computing desired parameters like distances and ages. The way the theorem is implemented in the project is developed further in section 2.2.

Chapter 2

Method

2.1 Galaxia

Galaxia (Sharma et al. 2011) is a program which can generate synthetic surveys of the Milky Way based on various parameters which can be adjusted by the user. The output catalogue of a survey is essentially a list of stars which were observed by a detector along measured and computed parameters, and their respective uncertainties. These parameters can be, for example, photometric (e.g. apparent magnitude), spectroscopic (e.g. effective temperature, mass, luminosity, distance), and astrometric (e.g. position, parallax). The difference between a real survey and a synthetic one is that for the latter we are generating virtual stars based on current working models of star populations of the Milky Way and we already know the values of their parameters with no uncertainty whatsoever.

The Galaxia code uses two different models to generate synthetic stars depending on their location in the galaxy. For the bulge and the two disks (thin and thick), the Besançon analytical model (Robin et al. 2003) is used, whereas the stellar halo uses an N-body model (particles modelled as collections of stars, Bullock & Johnston 2005). The equations used by the code can be seen in table A.4. It then uses stellar isochrones (evolution tracks of stars with the same age, as functions of mass, Marigo et al. 2008) to generate the parameters of each star in the survey. As highlighted by the tests in the original paper (Sharma et al. 2011, pp. 10-13), Galaxia yielded results in good agreement with its base model (Besançon) as well as various real measurements. However, there are still areas where it falls short, such as the omission of white dwarfs from the model since they are usually quite faint and rare, or the omission of chemical evolution within the stellar populations.

The initial parameters of each survey are given to the program in the form of a file. The most relevant parameters are illustrated in table A.1. It then simulates stars in a patch of sky (given by the area parameter) and generates a file containing the survey of stars for the given parameters, with information such as ages τ, positions in space, distances s (from which the parallaxes ϖ are obtained), metallicities [M/H], absolute magnitudes in the J, H, K_s spectral ranges, effective temperatures T_{eff}, and surface gravity $\log g$. These files are then opened in a python environment and the data contained inside is extracted

for analysis.

For the surveys used in this study, a limit on the apparent magnitude of stars was set to be between 9 and 12 in order to closely mimic the RAVE (Radial Velocity Experiment) survey (Kunder et al. 2017). The magnitudes obtained from the outputted models are absolute, however, and therefore a conversion had to be done to obtain the apparent magnitudes. The way this was done is shown by equation 2.1:

$$apparentMagnitude\_X = absoluteMagnitude\_X + \mu + X\_to\_V\_factor \cdot 3.1 \cdot exbv\_Schlegel \quad (2.1)$$

where μ is the distance modulus, *X_to_V_factor* is a multiplication factor specific to each photometric band relative to the V band (the values of which can be seen in eq. 2.8), and *exbv_Schlegel* is the extinction at the location of the star given by Schlegel dust maps (Schlegel, Finkbeiner, & Davis 1998).

2.2 BDASP

The data obtained from the Galaxia surveys was then analysed using the BDASP program (developed in the paper by McMillan et al. 2018) and "observed" parameters were obtained. The program takes in a number of parameters which are available for RAVE stars, such as galactic longitude and latitude, extinction at infinity according to Schlegel dust maps (Schlegel et al. 1998), as well as effective temperature, surface gravity, metallicity, apparent magnitudes in the J, H and K_s filters, and the parallax, along with the uncertainty in each of the values (except for the first 3 parameters). It then outputs computed values for almost all of the input parameters (except for the first 3) as well as for masses, ages, and distances.

2.2.1 General theory

The set of equations used by the program (as described in the paper by McMillan et al. 2018) begins from the Bayesian statement:

$$P(\text{model}|\text{data}) = \frac{P(\text{data}|\text{model})P(\text{model})}{P(\text{data})}, \quad (2.2)$$

where "data" contains the usual observables for a single star (as seen in table A.2), and "model" describes a star with modeled parameters (as seen in table A.3).

The P(data|model) probability is determined from assuming Gaussian (eq. 2.3) uncertainties on all inputs, and finding values for the stellar parameters and absolute magnitudes of the model star by using isochrones (Marigo et al. 2008). A more detailed description is found in the paper by McMillan et al. 2018. P(model) is the prior, and P(data) is a normalization constant which can be ignored.

$$G(x, \mu, \sigma) = \frac{1}{\sqrt{2\pi\sigma^2}} \exp\left(\frac{(x-\mu)^2}{2\sigma^2}\right), \quad (2.3)$$

Therefore, a general form of the obtained probability is given by:

$$\begin{aligned} P(\text{model}|\text{data}) &\propto P(\text{data}|\text{model}) \times P(\text{model}) \\ \Leftrightarrow P(\mathcal{M}, \tau, [\text{M/H}], s, A_V|\,\text{data}) &\propto \prod_i G(O_i^T(\mathcal{M}, \tau, [\text{M/H}], s, A_V), O_i, \sigma_i) \\ &\quad \times P(\mathcal{M}, \tau, [\text{M/H}], s, A_V|l, b) \end{aligned} \tag{2.4}$$

where O_i, σ_i are the observables and their uncertainties, O_i^T are the theoretical values obtained from the isochrones and extinction, and $P(\mathcal{M}, \tau, [\text{M/H}], s, A_V|l, b)$ is the prior (described in section 2.2.2).

2.2.2 Prior

"The prior reflects some elements of our existing understanding of the Galaxy, at the cost of possibly biasing us against some results that run counter to our expectations..."(McMillan et al. 2018)

It can be written as:

$$\begin{aligned} P(\text{model}) &= P(\mathcal{M}, \tau, [\text{M/H}], s, A_V|l, b) \\ &= P(\mathcal{M}) \times P(A_V|\,s, l, b) \times P(s, [\text{M/H}], \tau|\,l, b) \end{aligned} \tag{2.5}$$

where the prior on initial mass is an initial mass function (IMF) by Kroupa 2001, modified by Aumer & Binney 2009:

$$P(\mathcal{M}) \propto \begin{cases} 0 & \text{if } \mathcal{M} < 0.1\,M_\odot \\ \mathcal{M}^{-1.3} & \text{if } 0.1\,M_\odot \leq \mathcal{M} < 0.5\,M_\odot, \\ 0.536\,\mathcal{M}^{-2.2} & \text{if } 0.5\,M_\odot \leq \mathcal{M} < 1\,M_\odot, \\ 0.536\,\mathcal{M}^{-2.519} & \text{otherwise.} \end{cases} \tag{2.6}$$

The prior in terms of the extinction is described by a Gaussian in $\ln A_v$ around an expected value $\ln A_V^{\text{pr}}(s, l, b)$ which varies with the model star's position:

$$P(A_V|s, l, b) = G(\ln A_V,\ \ln(A_V^{\text{pr}}(s, l, b)),\ \sqrt{2}). \tag{2.7}$$

For conversion between the different bands, the extinction are taken from Rieke & Lebofsky 1985 to be:

$$\begin{aligned} A_J &= 0.282 A_V \\ A_H &= 0.175 A_V \\ A_{K_s} &= 0.112 A_V, \end{aligned} \tag{2.8}$$

The last term in the prior gives the probability of finding a star at a given position, with a certain age τ and metallicity [M/H]. A factor s^2 accounts for the conical shape of

the surveyed volume. Therefore, the term is written as:

$$P(s, [\mathrm{M/H}], \tau | \, l, b) \propto s^2 \sum_{i=1}^{3} N_i P_i([\mathrm{M/H}]) \, P_i(\tau) \, P_i(\mathbf{r}), \tag{2.9}$$

where $i = 1, 2, 3$ correspond to the thin disk, thick disk and halo, and r is the position of the star relative to the galactic centre.

In this project, three different priors were used, taken from McMillan et al. 2018, in order to avoid a dependency on the choice of prior. They each take into account different assumptions about the distribution of stars which affect the last term (i.e. eq. 2.9). The terms common to all 3 priors for each of the three galactic components describe the density distribution of the stars, and are given by:

Thin disc ($i = 1$):

$$P_1(\mathbf{r}) \propto \exp\left(-\frac{R}{R_d^{\mathrm{thin}}} - \frac{|z|}{z_d^{\mathrm{thin}}}\right) \tag{2.10}$$

Thick disc ($i = 2$):

$$P_2(\mathbf{r}) \propto \exp\left(-\frac{R}{R_d^{\mathrm{thick}}} - \frac{|z|}{z_d^{\mathrm{thick}}}\right) \tag{2.11}$$

Halo ($i = 3$):

$$P_3(\mathbf{r}) \propto r^{-3.39} \tag{2.12}$$

Density prior

We first look at the 'Density' prior, for which the priors on age and metallicity are set to be uniform. A maximum age of 13.8 Gyr is set, while the metallicity limits are set by the isochrones (Marigo et al. 2008). Thus, we have:

$$\begin{aligned} P_1([\mathrm{M/H}]) = P_2([\mathrm{M/H}]) = P_3([\mathrm{M/H}]) = \text{const.} \\ P_1(\tau) = P_2(\tau) = P_3(\tau) = \text{const.} \end{aligned} \tag{2.13}$$

Age prior

We can use a more informative prior, where $P(\tau)$ is not uniform, but instead assumes that the star formation rate in the galaxy has declined over time. Thus,we have:

$$P_1(\tau) = P_2(\tau) = P_3(\tau) \propto \exp(0.119\,\tau/\mathrm{Gyr}) \quad \text{for } \tau \leq 10\,\mathrm{Gyr} \tag{2.14}$$

Metallicity prior

Finally, we can use an even more informative prior which employs the assumptions that metal rich and/or young stars are most common in the galactic plane. This gives us priors on metallicity and age described by:

Thin disc ($i = 1$):

$$\begin{aligned} P_1([\mathrm{M/H}]) &= G([\mathrm{M/H}], 0, 0.2), \\ P_1(\tau) &\propto \exp(0.119\,\tau/\mathrm{Gyr}) \quad \text{for } \tau \leq 10\,\mathrm{Gyr} \end{aligned} \tag{2.15}$$

Thick disc ($i = 2$):

$$\begin{aligned} P_2([\mathrm{M/H}]) &= G([\mathrm{M/H}], -0.6, 0.5), \\ P_2(\tau) &\propto \text{uniform in range } 8 \leq \tau \leq 12\,\mathrm{Gyr} \end{aligned} \tag{2.16}$$

Halo ($i = 3$):

$$\begin{aligned} P_3([\mathrm{M/H}]) &= G([\mathrm{M/H}], -1.6, 0.5) \\ P_3(\tau) &\propto \text{uniform in range } 10 \leq \tau \leq 13.7\,\mathrm{Gyr} \end{aligned} \tag{2.17}$$

2.2.3 Alternative initial mass functions (IMFs)

BDASP was also modified to use two other IMFs. The first one is a slightly modified version of the Chabrier IMF (Romano et al. 2005):

$$\varphi_{\mathrm{C}}(\mathcal{M}) = \begin{cases} 0 & \text{if } \mathcal{M} < 0.1\,M_{\odot}, \\ \frac{A}{\mathcal{M}} \exp\left(-\frac{(\log \mathcal{M} - \log \mathcal{M}_c)^2}{2\sigma^2}\right) & \text{if } 0.1\,M_{\odot} \leq \mathcal{M} < 1\,M_{\odot}, \\ B\,\mathcal{M}^{-1.3} & \text{if } \mathcal{M} \geq 1\,M_{\odot}, \end{cases} \tag{2.18}$$

where $A = 0.85$, $B = 0.24$, $\mathcal{M}_c = 0.079$ and $\sigma = 0.69$

The second IMF is the one used by Galaxia in its models, as seen in table A.4. However, it only applies for the stars in the thin disc, and thus might provide erroneous results for stars not belonging to it:

$$\varphi_{\mathrm{G}}(\mathcal{M}) \propto \begin{cases} \mathcal{M}^{-1.6} & \text{if } \mathcal{M} < 1\,M_{\odot} \\ \mathcal{M}^{-3} & \text{if } \mathcal{M} \geq 1\,M_{\odot}, \end{cases} \tag{2.19}$$

A comparison between the 3 different IMFs that were used is given by fig. 2.1.

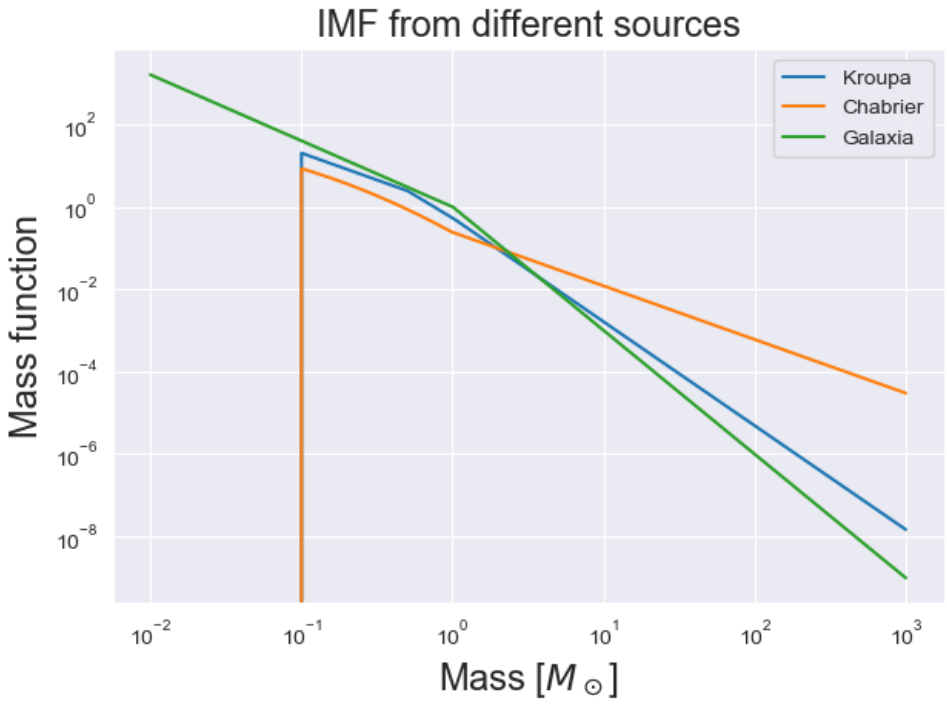

Figure 2.1: Comparison between the different types of IMF used by BDASP.

Chapter 3

Results & Discussion

In this section, the comparison between the original and computed data for different stellar parameters as well as different priors is presented in terms of histograms in order to see if we are over-estimating (denoted in dark blue, negative values) or under-estimating (denoted in red, positive values) the values of the observables. A one-dimensional histogram illustrates the distribution of a stellar parameter as compared to a normal distribution of standard deviation 1 and a mean of 0. This is to check how close the computed values are to their true counterparts. A median and inter-quartile range (IQR) value is computed for each histogram with a central value of 0 for the median and a spread value of 1 for the IQR indicating a perfect match (with the IQR being scaled relative to $1.349\sigma = 1.349$). Furthermore, a two-dimensional histogram overlayed on a surface gravity vs. effective temperature diagram is meant to show which types of stars provide the differences from the expected values depending on their location in the diagram. This is a variation on the Hertzsprung-Russel diagram, and its features describe different families of stars (main-sequence branch, giant and hypergiant branch).

A number of around 53200 "fake stars" have been used in each variation of the model generated by Galaxia with small variations due to unreasonable computed uncertainties by BDASP (which required culling some entries). In order to simulate real observations, uncertainties were added to the input data which went into BDASP. They were taken as the average of uncertainties for the observations found by RAVE in the fifth data release (Kunder et al. 2017), and their values can be found in table 3.1.

The data provided by the Galaxia model was then analysed by BDASP using the 3 different mentioned priors as well as the 3 different IMFs (described in section 2.2 and seen in fig. 2.1). The stellar parameters being compared in each case are the age, surface gravity, distance, mass, and effective temperature. The different priors were tried in order to avoid being biased to the choice of prior. The different IMFs were tried since unexpected results were obtained for the stellar masses (which are directly affected by the IMFs). A fourth set of measurements and calculated parameters was done using the 3 different priors, all with the Kroupa IMF, and with a smaller value of the parallax uncertainty (0.05 mas) to see if it improved the results in any way.

Table 3.1: Uncertainties used to build the mock catalogue of stars. The values are averages from measurements taken from the RAVE DR5 survey (Kunder et al. 2017).

Parameter	Symbol	Uncertainty value	Unit
Effective temperature	T_{eff}	84.9083	K
Surface gravity	$\log g$	0.1844	dex
Metallicity	[M/H]	0.1170	dex
Parallax	ϖ	0.3967	mas
J-band magnitude	J	0.0248	dex
H-band magnitude	H	0.0300	dex
K_s-band magnitude	K_s	0.0235	dex

3.1 Density prior

3.1.1 Kroupa IMF

We start with using the Density prior and the Kroupa IMF when computing the parameter values using BDASP. The Density prior, aptly named, only takes into account the density distribution of stars in the galaxy. The Kroupa IMF, as seen in fig. 2.1, excludes very low mass stars ($< 0.1\,M_\odot$) and follows a power law distribution for the rest, broken up into 3 zones (as seen in eq. 2.6). We then look at the five parameters of interest: ages, surface gravities, distances, stellar masses and effective temperatures.

For the age values, there seems to be a slight systematic overestimation and a moderate spread as indicated by the median and IQR values in fig. 3.1. Looking at the 2D histogram, there is a narrow band along the main-sequence, leading upwards towards the giant branch in which there is good agreement between the true and computed data. However, as one can see, there are areas like the giant and supergiant branch in which the values are moderately underestimated. Along the main sequence, a variation in surface gravity for a given temperature introduces large overestimation/underestimation in the age values which suggests that they are quite sensitive to surface gravity. This also seems to hold for most of the other parameters.

When it comes to surface gravity, there is a slight systematic underestimation, although the spread is considerably lower, as seen in fig. 3.2. The giant branch seems to be responsible for most of that. For more massive main-sequence stars there is a moderate overestimation.

Next, we have the distance values, which seem to be overestimated slightly according to fig. 3.3. We see that the giant branch is once again the one affected the most. Otherwise main-sequence stars' distances are once again in good agreement within a narrow band.

The stellar masses seem to be greatly underestimated according to fig. 3.4. It seems to affect the main-sequence branch mostly which is surprising as the stars in this branch should be more predictable than the others and the theory that we have seems to describe

them decently. The most affected ones appear to be cool dwarfs. There is also a slight overestimation in the masses of giants.

Finally, the comparison for the effective temperatures can be seen in fig. 3.5. There seems to be a slight underestimation overall, but the dispersion is very low. Giants (possibly super- or hypergiants only) seem to have some moderate underestimation in the effective temperatures, while cool dwarfs are being overestimated.

Overall, the results are showing that there are indeed differences between the true and calculated data, some quite significant like in the case of ages and stellar masses. For most cases, the culprits seem to be stars in the giant branch and in some, like ages and stellar masses, even cool dwarfs. The age and mass comparison have a larger spread than the other cases, with the mass comparison also having a large median value suggesting that we are underestimating the mass values by about half a standard deviation. Thus, in the following sections we continue to explore these differences by trying out different IMFs and priors.

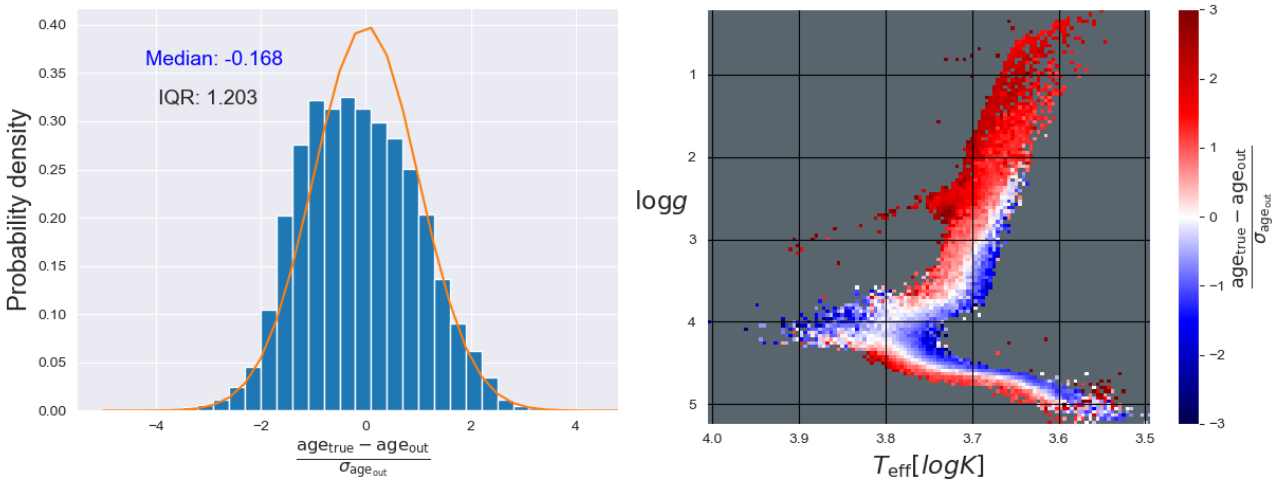

Figure 3.1: Comparison between true and calculated values for the age of the virtual stars for the Kroupa IMF. In the left figure we observe a moderate spread, and a systematic overestimation of the calculated values. In the right figure we can observe the sources of over-/underestimation. In this case it seems stars which have an early turn-off from the main sequence (or even some late outliers) denoted by the dark blue zones are the main culprits. Stars in the giant branch, on the contrary, seem to have their age underestimated (denoted by the red area at the top).

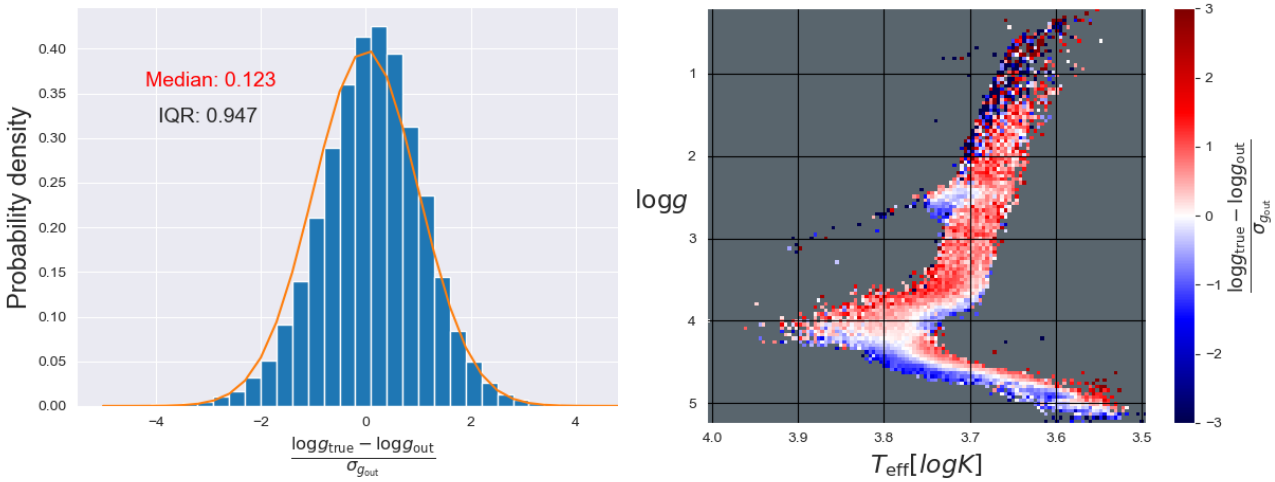

Figure 3.2: Comparison between true and calculated values for the surface gravity of the virtual stars for the Kroupa IMF. In the left figure we can see that the distribution is very close to the expected curve, with a slightly lower spread and a median which suggests a systematic underestimation. We can see in the right figure that it is mostly stars in the giant branch which seem to suffer from this, along with some lower mass main-sequence stars.

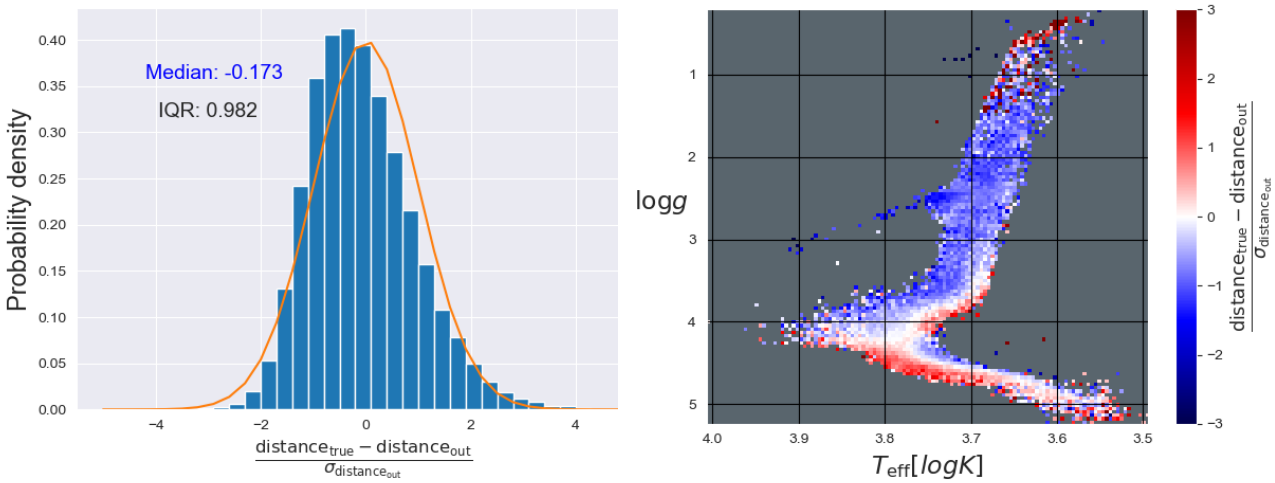

Figure 3.3: Comparison between true and calculated values for the distances of the virtual stars for the Kroupa IMF. In the left figure we observe that the distribution has a slightly lower spread than expected (in fact it seems to be the closest to the expected curve among the parameters measured with the Kroupa IMF and the Density prior). We also see that the values are overestimated from the median value. Looking at the right figure we see that the culprits are once again stars from the giant branch.

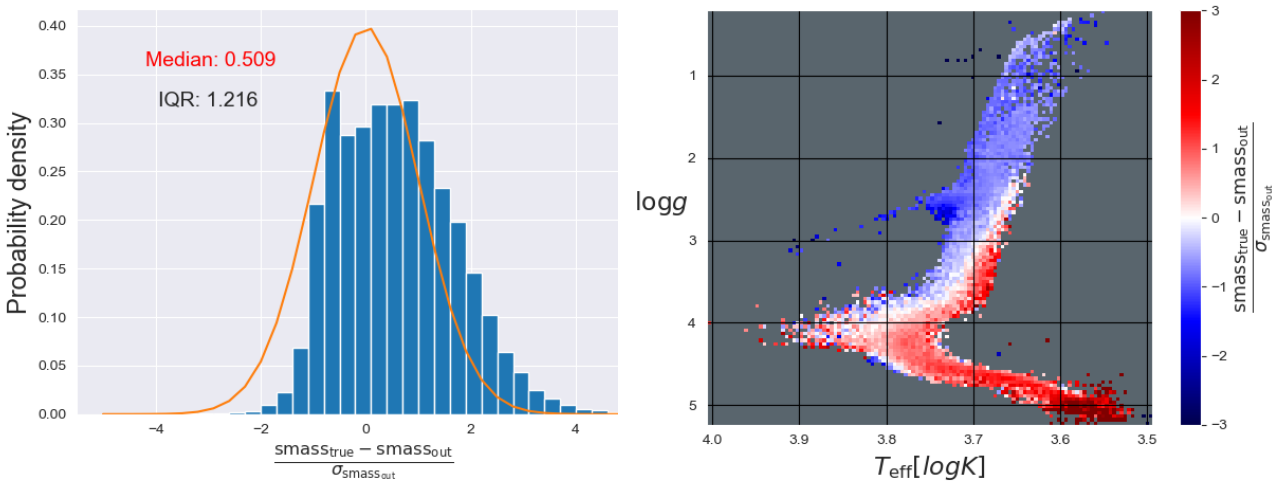

Figure 3.4: Comparison between true and calculated values for the masses of the virtual stars for the Kroupa IMF. In the left figure we see that the distribution is moderately different from the expected curve. With the largest spread value and systematic underestimation among the parameters, this indicates a significant issue. We can see in the right figure that the ones affected are in fact main-sequence stars, with the most affected being cool dwarf stars. In the giant branch we instead see an overestimation in masses.

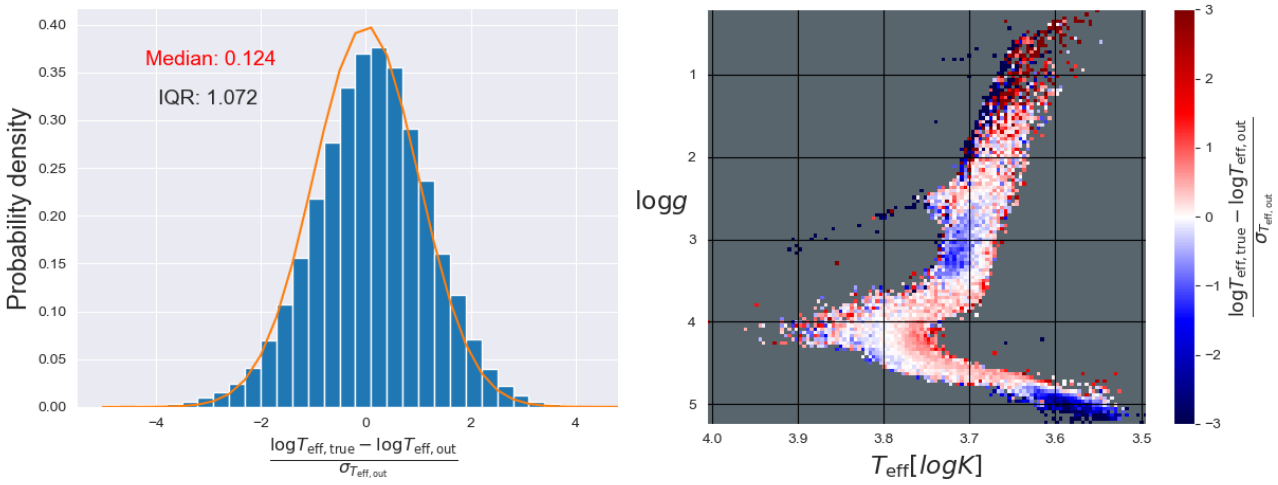

Figure 3.5: Comparison between true and calculated values for the effective temperatures of the virtual stars for the Kroupa IMF. In the left figure we see that the distribution is very close to the expectation, with a slightly larger spread and a slight underestimation in temperatures. On the right we see that the most significantly affected regions are the very end of the giant branch (providing temperature underestimation; possibly hypergiants) and low-mass main-sequence stars (providing temperature overestimation).

3.1.2 Chabrier IMF

From the results in the previous section we see that the masses are systematically underestimated by a large amount. Since these are directly affected by the IMF, we now try using the Chabrier IMF. As seen in fig. 2.1, it shares the same cut-off for very low-mass stars as the Kroupa IMF, while dropping off less quickly for larger mass stars.

However, we find that there is almost no difference in the parameter values when using the Chabrier IMF. This is somewhat surprising since one would expect higher masses (although it does seem that there is a slight increase in underestimation of stellar masses according to fig. 3.6).

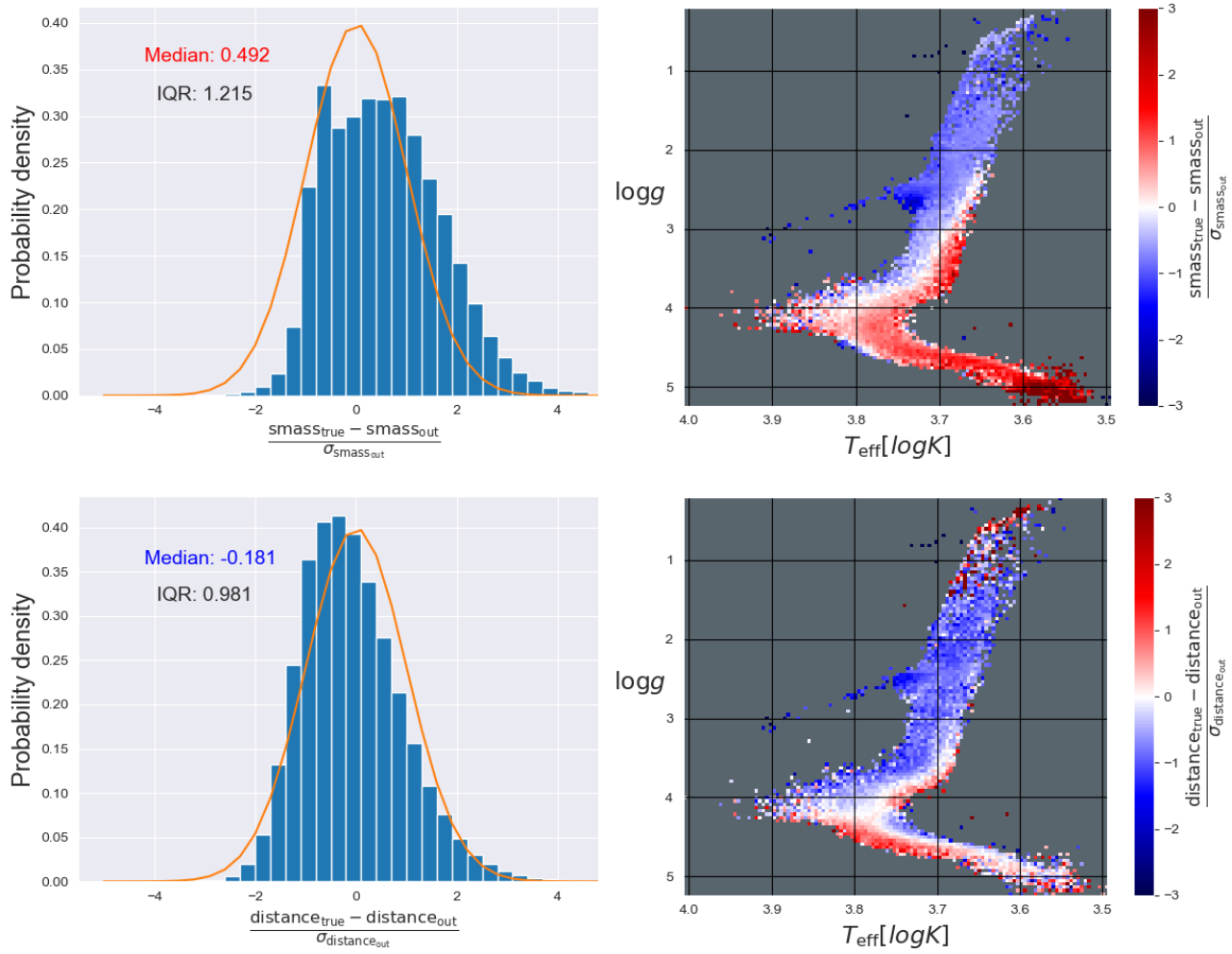

Figure 3.6: *Top:* Comparison between true and calculated values for the masses of the virtual stars for the Chabrier IMF. Only a very slight decrease in the median value is observed when compared to the values for the Kroupa IMF. Apart from that, the features in the right figure are identical to the previous IMF case. *Bottom:* Comparison between true and calculated values for the distances of the virtual stars for the Chabrier IMF. Similarly, almost no differences for this distribution compared to the previous case.

3.1.3 Galaxia IMF

Finally, for this section we look to directly copy the IMF used by Galaxia, in order to see if the previous two IMFs are faulty in some way. One would expect very little to no deviations from the true values if we were to use the same IMF as used by the model which generated the virtual stars. However, we find that this is not the case (fig. 3.8) and the values for the masses are still systematically wrong, with almost no difference to the other two IMFs.

Compared to the other two IMFs, the Galaxia IMF does not have a cut-off for the smallest masses, as seen in fig. 2.1. There are also two formulas, depending whether the star is in the thin or the thick disk (according to table A.4). The IMF used by BDASP only contained the formula for the thin disk, as seen in eq. 2.19. Therefore, in order to see how large of an effect that had on the stellar mass, a split of the data was done between stars younger than 11 Gyr and older stars.

The results for the split are shown in fig. 3.7. The masses for older stars (which were about 680 out of the total number of 53200 stars) seem to be indeed more underestimated. However, when looking at the young stars, they are still suffering from the same issue, with little apparent impact from excluding the old stars. Thus there must be some other cause for the inaccuracy which affects all masses.

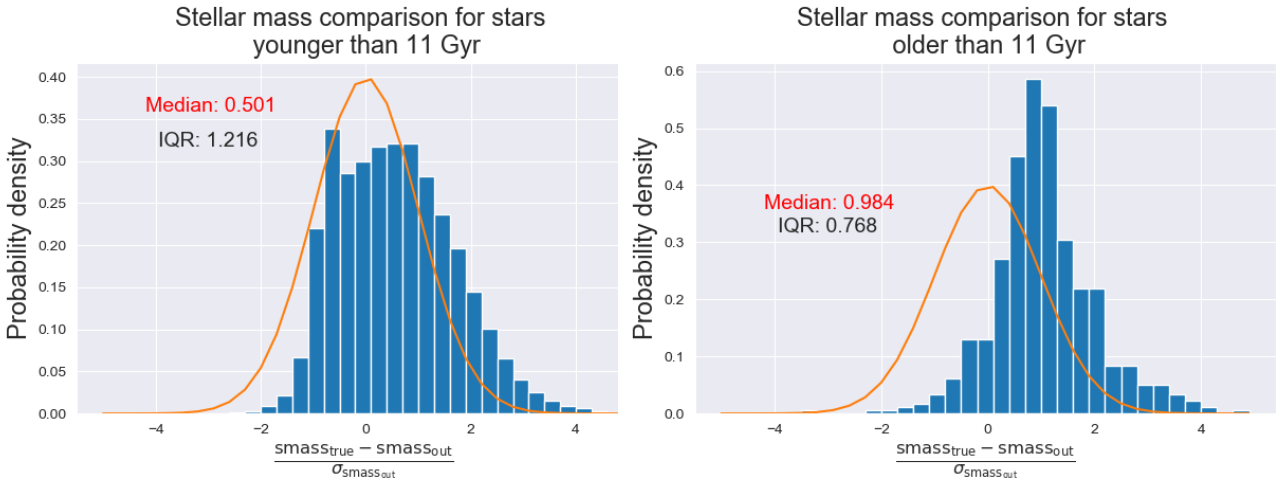

Figure 3.7: Comparison between true and calculated values for the masses of the virtual stars, using the Galaxia IMF. In the left figure we observe the masses for young stars (at the cut-off used by Galaxia in table A.4). There seems to have been almost no effect in sorting out the old stars, though perhaps it is to be expected since they were in the minority. On the right we see the distribution of masses for the old stars which has a very small spread and a very large median. This is also to be expected since for the thick disk older stars the slope of the IMF is much less steeper which would introduce higher masses and thus increase the underestimation.

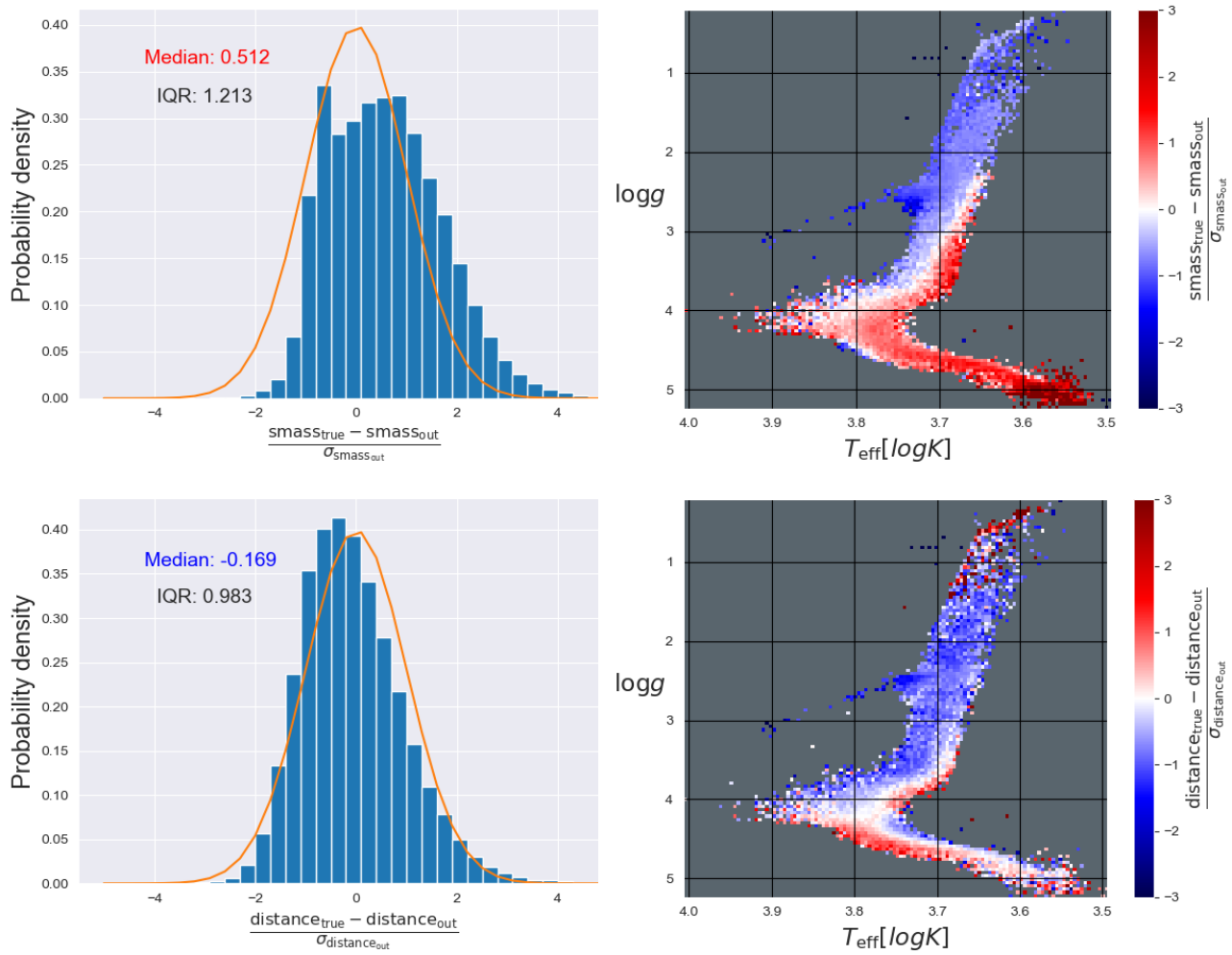

Figure 3.8: *Top:* Comparison between true and calculated values for the masses of the virtual stars for the Galaxia IMF. Only another small variation in the median value when compared to the two previous cases. The overall features in the right figure remain unchanged. *Bottom:* Comparison between true and calculated values for the distances of the virtual stars for the Galaxia IMF. Similarly, almost no differences for this distribution compared to the previous cases.

3.2 Age prior

Changing the IMF prior did not bring our results in line with our expectations. We therefore look at changing the other elements in our prior. The Age prior includes, on top of the density prior, a non-uniform prior on the stellar age, as described in section 2.2.2 by eq. 2.14.

3.2.1 Kroupa IMF

When using the Age prior, there is a significant increase in overestimation of the age values, as seen in fig. 3.9. The dispersion is still large and the contrast between the zones on the 2D histogram increases. Perhaps this is due to using the same form for both the thin and thick disk stars, as described in section 2.2.2. Surface gravity underestimation seems to slightly increase with this prior as well (fig. 3.10). Distance is slightly more overestimated (fig. 3.11). Stellar mass is still greatly underestimated, with an even larger value (fig. 3.12). Finally, effective temperature is still reasonably good (albeit with a slightly larger median value) as seen in fig. 3.13.

Overall, whatever tendencies the measurements had with the Density prior seem to have been amplified in moderate amounts. Again, this might be due to treating stars from the different galactic components with the same formula. Or perhaps there might be some underlying issue with the assumption that star formation rate decreases with the age of the galaxy. Once again, in the following sections, we explore the changes brought by trying the other two IMFs, since the stellar masses issue still persists.

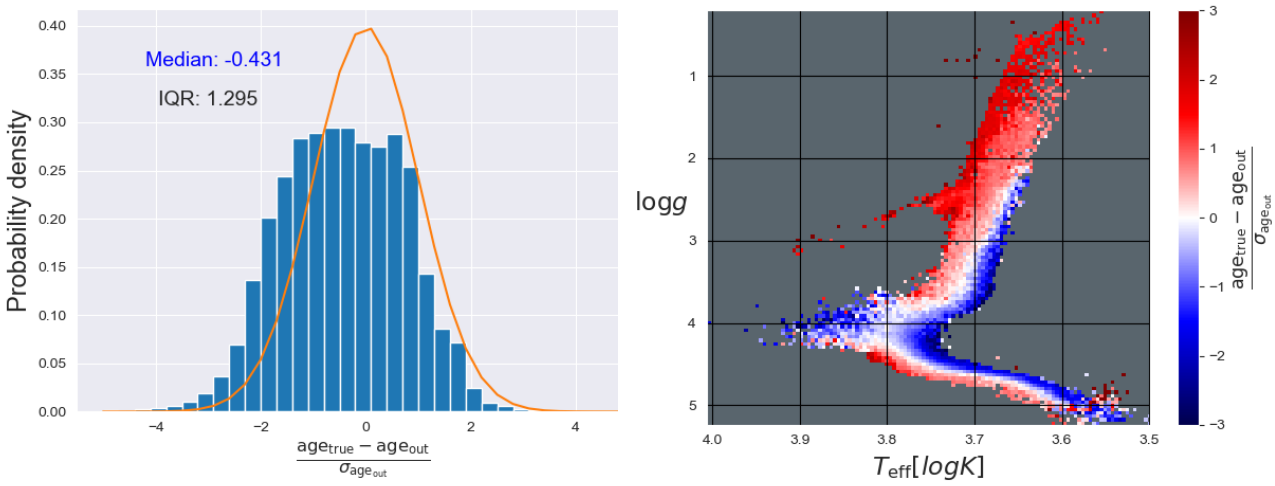

Figure 3.9: Comparison between true and calculated values for the age of the virtual stars for the Kroupa IMF., using the Age prior. In the left figure we see that the spread of the distribution has worsened compared to the Density prior (fig. 3.1). The median value has also greatly decreased which gives a large systematic overestimation of ages. On the right we see that the zones affected remain the same as in the previous prior case, with a slightly increased contrast between them.

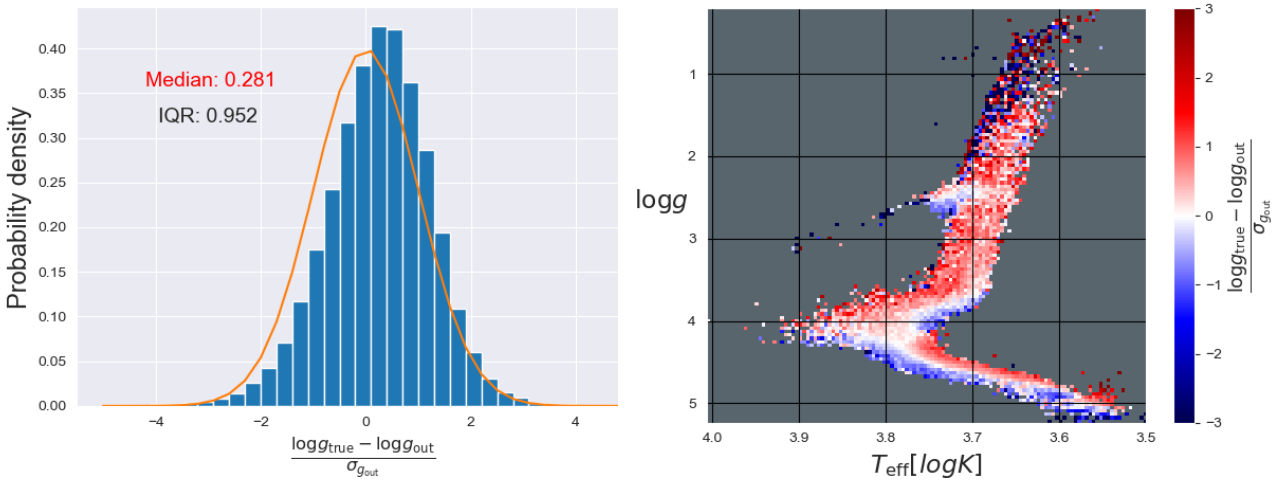

Figure 3.10: Comparison between true and calculated values for the surface gravity of the virtual stars for the Kroupa IMF, using the Age prior. In the left figure we see that the distribution has mostly the same spread as with the previous prior (fig. 3.2), while the median value has almost doubled. On the right the features are mostly the same, albeit reflecting the increase in overall underestimation.

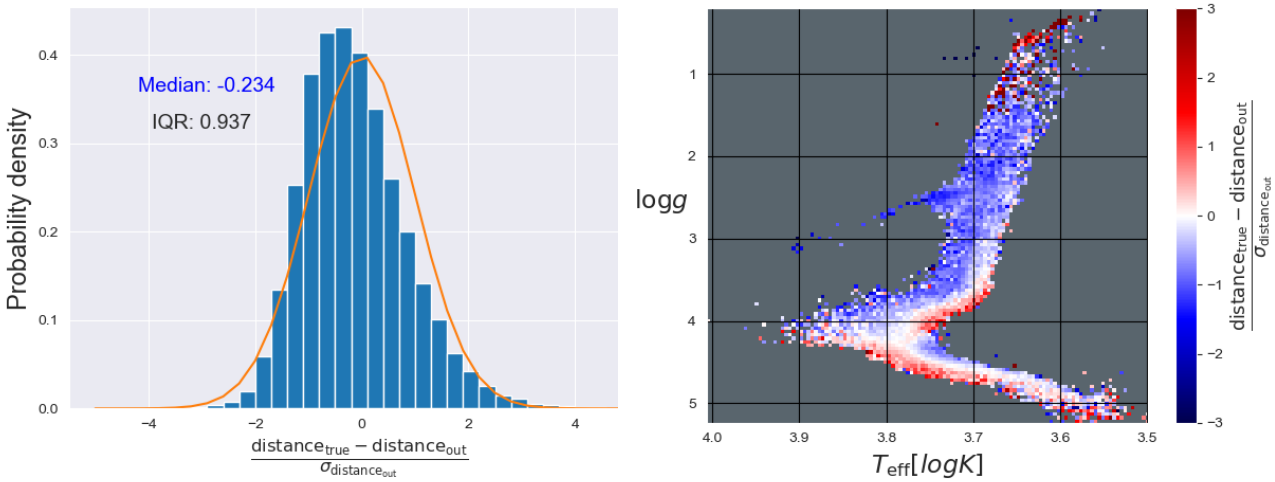

Figure 3.11: Comparison between true and calculated values for the distances of the virtual stars for the Kroupa IMF, using the Age prior. On the left, the distribution is mostly the same as in the previous case, albeit with an almost doubled median value. On the right we can see that the features are overall the same as before, now slightly less red, indicating the increase in overall overestimation.

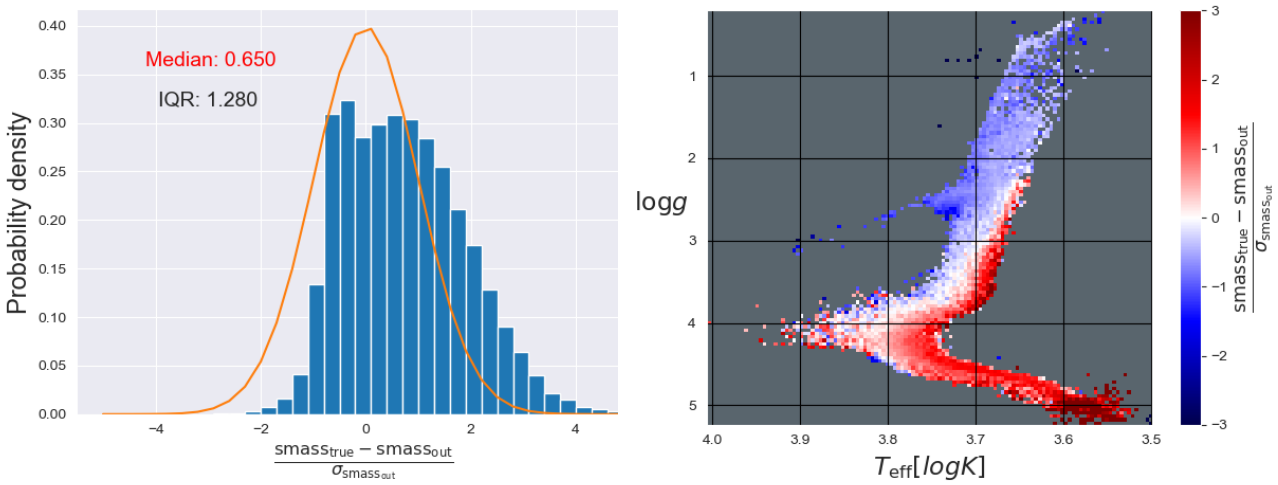

Figure 3.12: Comparison between true and calculated values for the masses of the virtual stars for the Kroupa IMF, using the Age prior. On the left we can see that the distribution has slightly worsened compared to before (fig. 3.4). A higher median value and spread are reflected on the right figure in an overall reddening of the features. However, the affected stars are the same as before.

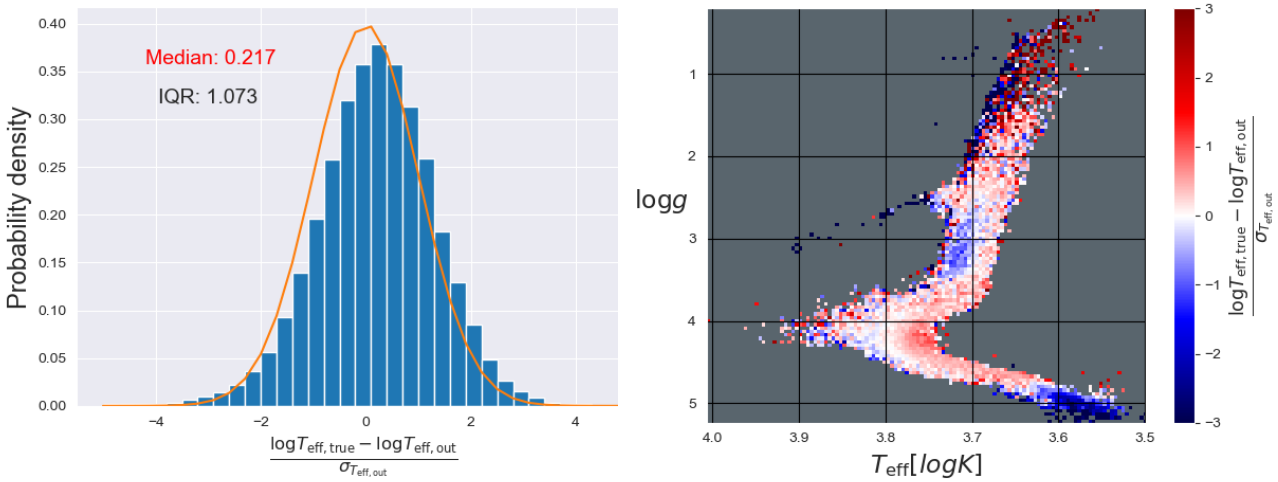

Figure 3.13: Comparison between true and calculated values for the effective temperatures of the virtual stars for the Kroupa IMF, using the Age prior. On the left the distribution is mostly the same, with an almost doubled median. On the right we have the same features as in the previous case with almost no changes.

3.2.2 Chabrier IMF

Similar to the previous prior, there are almost no differences between the Kroupa and the Chabrier IMF, however compared to the previous prior, as mentioned before, the tendencies of the parameter comparison have been moderately (and even greatly) amplified, with some cases such as the age median (fig. 3.14) almost tripling in value.

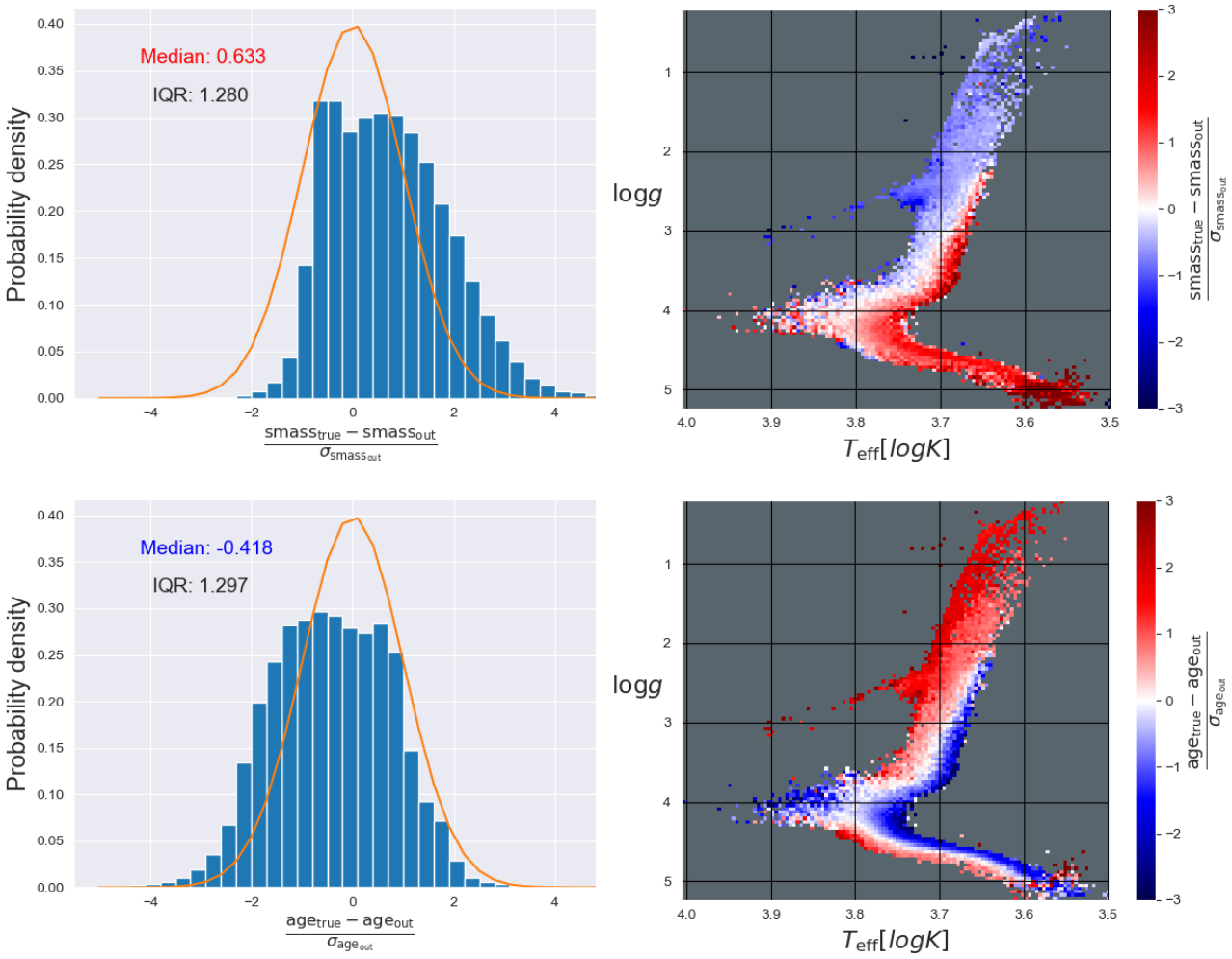

Figure 3.14: *Top:* Comparison between true and calculated values for the masses of the virtual stars for the Chabrier IMF, using the Age prior. On the left we can see that the distribution of the masses is still being systematically underestimated, even more so than previous cases. Otherwise, there are no immediately obvious changes on the right figure, with the features staying the same. *Bottom:* Comparison between true and calculated values for the ages of the virtual stars for the Chabrier IMF, using the Age prior. On the left we can see that the median value has almost tripled compared to before. On the right the features stay mostly the same.

3.2.3 Galaxia IMF

Once again, almost no differences at all between the IMFs, but an amplification of the median value between priors for all of the parameters.

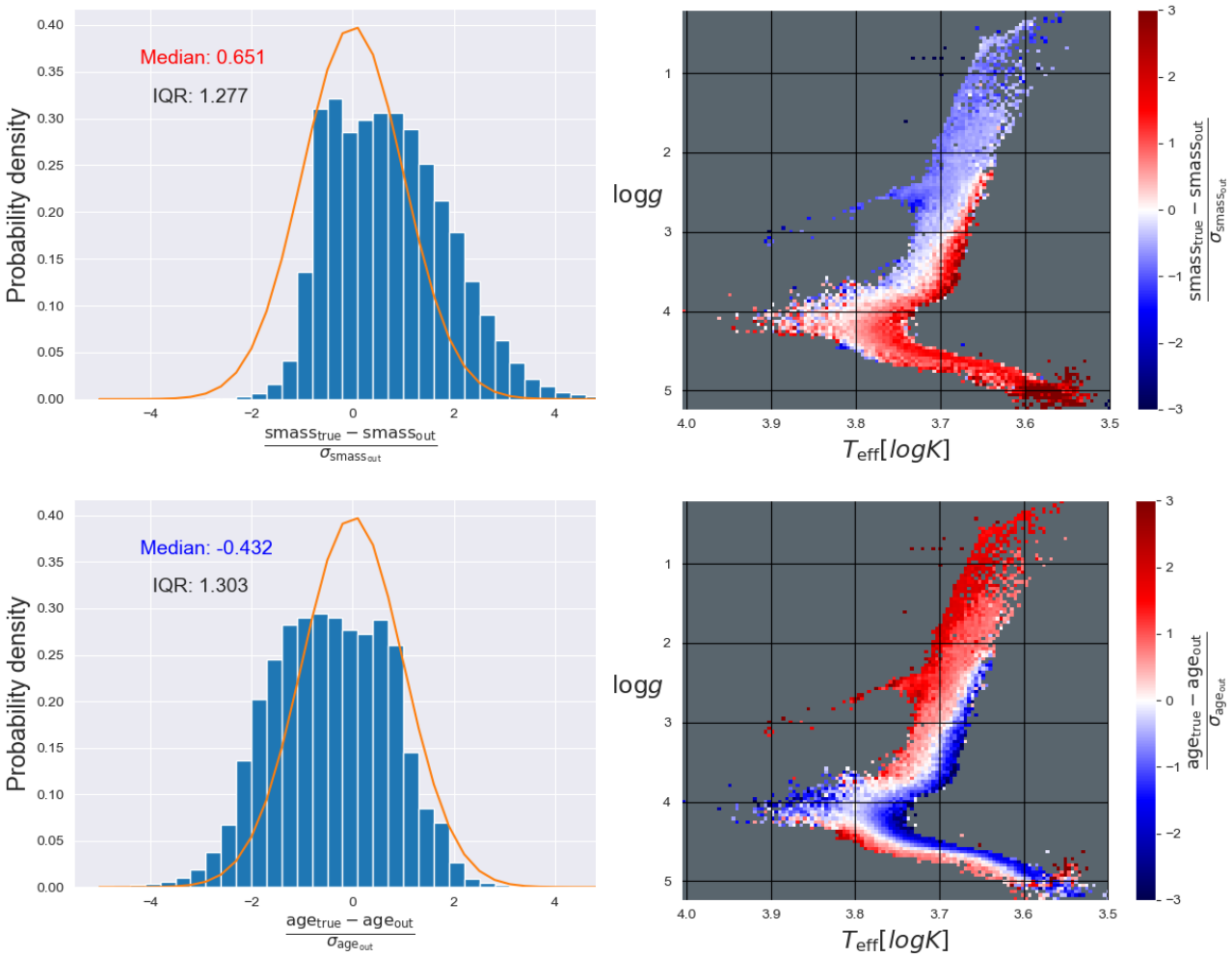

Figure 3.15: *Top:* Comparison between true and calculated values for the masses of the virtual stars for the Galaxia IMF, using the Age prior. On the left we can see that the distribution of the masses is still being systematically underestimated, even more so than previous cases. Otherwise, there are no immediately obvious changes on the right figure, with the features staying the same. *Bottom:* Comparison between true and calculated values for the ages of the virtual stars for the Galaxia IMF, using the Age prior. On the left we can see that the median value has almost tripled compared to the previous prior. On the right the features stay mostly the same.

3.3 Metallicity prior

Next, we turn to the Metallicity prior (described in section 2.2.2) to see if we can obtain better results. The Metallicity prior assumes that metal rich and/or young stars are most commonly found in the galactic plane, and thus provides non-uniform priors for metallicity and age, specific to each galactic component. This is possibly still slightly different from what Galaxia assumes (since Galaxia uses the age-metallicity relation according to Sharma et al. 2011, while the Metallicity prior does not; Galaxia does not assume metal rich stars are confined mostly to the galactic plane), however it is probably closer to reality.

The results obtained by using this prior are somewhat strange (in the case of ages), but overall mostly better than for the other two priors. For ages, regardless of the IMF used, there seems to be a rather large peak at what seems to be 1 standard deviation (σ) difference between the true values and the calculated ones (e.g. fig. 3.16). Perhaps this might have something to do with the more rigid thresholds this prior employs, lumping together otherwise slightly different values. The effect of these thresholds can also be seen in the 2D histograms, with a sharper delimitation between the different coloured zones.

3.3.1 Kroupa IMF

As mentioned previously, the age comparison yielded peculiar results (fig. 3.16). However, disregarding the peak at 1 standard deviation, overall it is still being overestimated slightly more than the Density prior, but less than the Age prior. As for the other parameters, they all seem to have improved in accuracy, with overall less spread and only slightly less over-/underestimation (figures 3.17 - 3.20). There also seem to be less sharp gradients in the $\log g/T_{\text{eff}}$ plane.

In spite of using this prior, however, the systematic issue with the stellar masses still persists. We therefore, once again, try different IMFs to see if they have any effect.

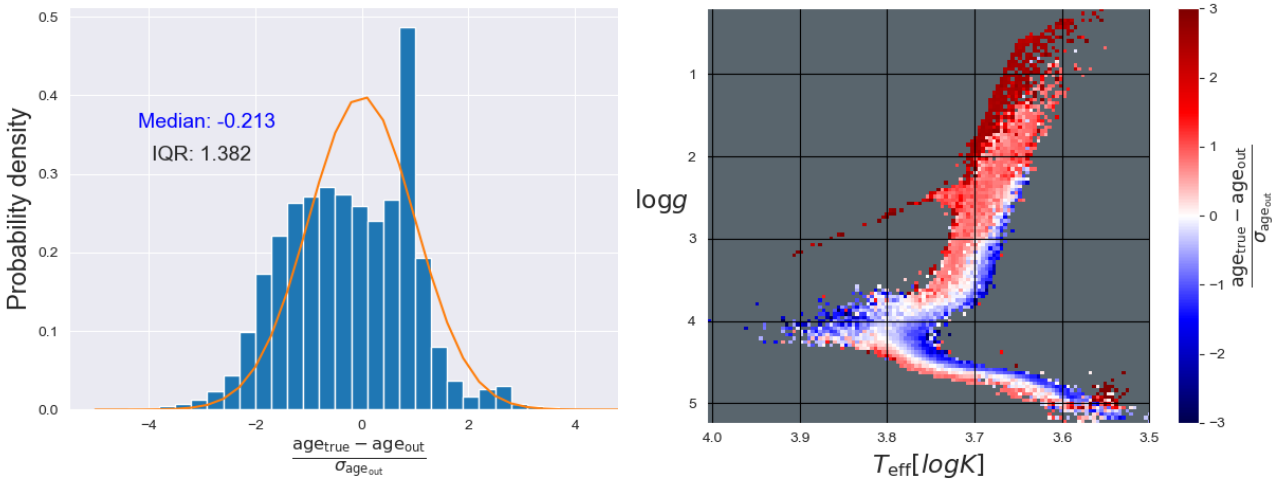

Figure 3.16: Comparison between true and calculated values for the age of the virtual stars for the Kroupa IMF, using the Metallicity prior. On the left we observe an even larger spread of the distribution than before, with a peculiar peak at a value of about 1 standard deviation. This seems to suggest that we are severely underestimating some large number of stars by 1 standard deviation. This is probably made clearer when looking at the right figure, and observing the giant branch. Overall the giant branch seems to be the one affected once again, with the vast majority falling under 1 standard deviation. The higher ends of the branch seem to be also vastly underestimated.

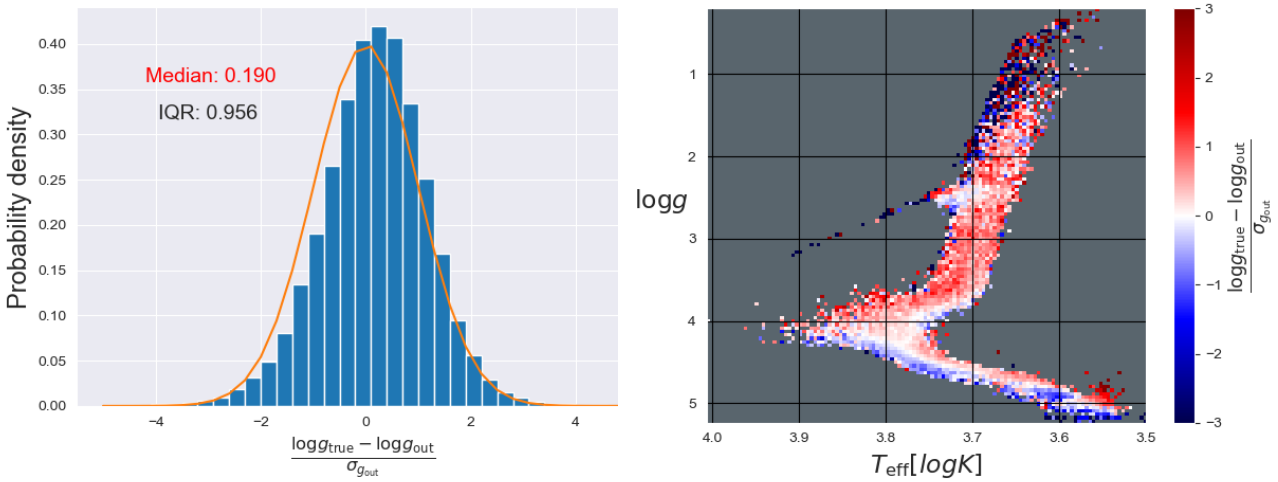

Figure 3.17: Comparison between true and calculated values for the surface gravity of the virtual stars for the Kroupa IMF, using the Metallicity prior. On the left we observe the distribution of surface gravity values being very close to expectations, with a slight systematic underestimation. On the right, we see that the giant branch is mostly the one responsible.

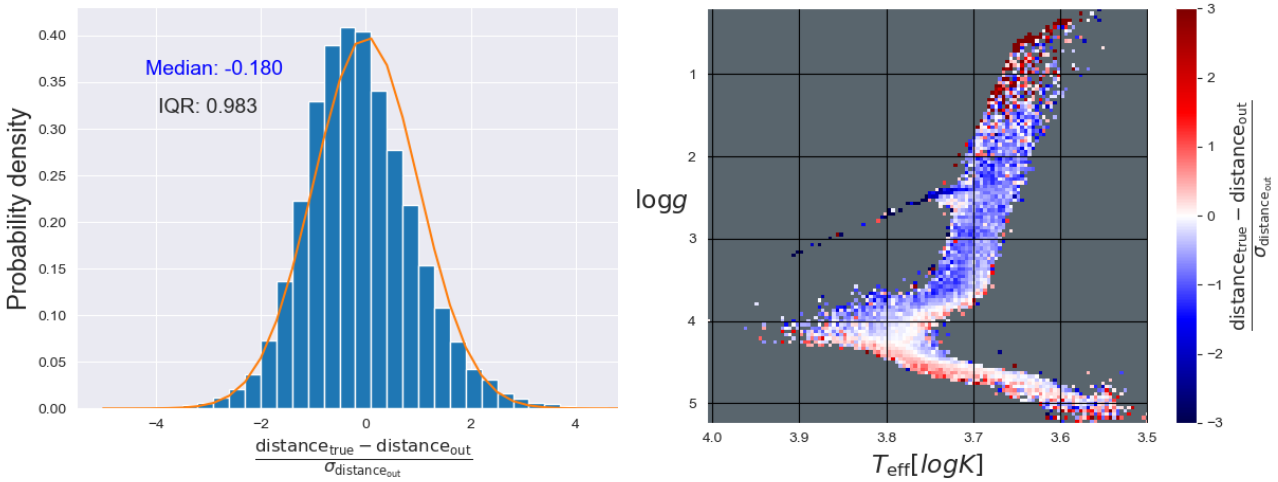

Figure 3.18: Comparison between true and calculated values for the distances of the virtual stars for the Kroupa IMF, using the Metallicity prior. The distribution on the left is mostly unchanged from previous cases, as is the one on the right.

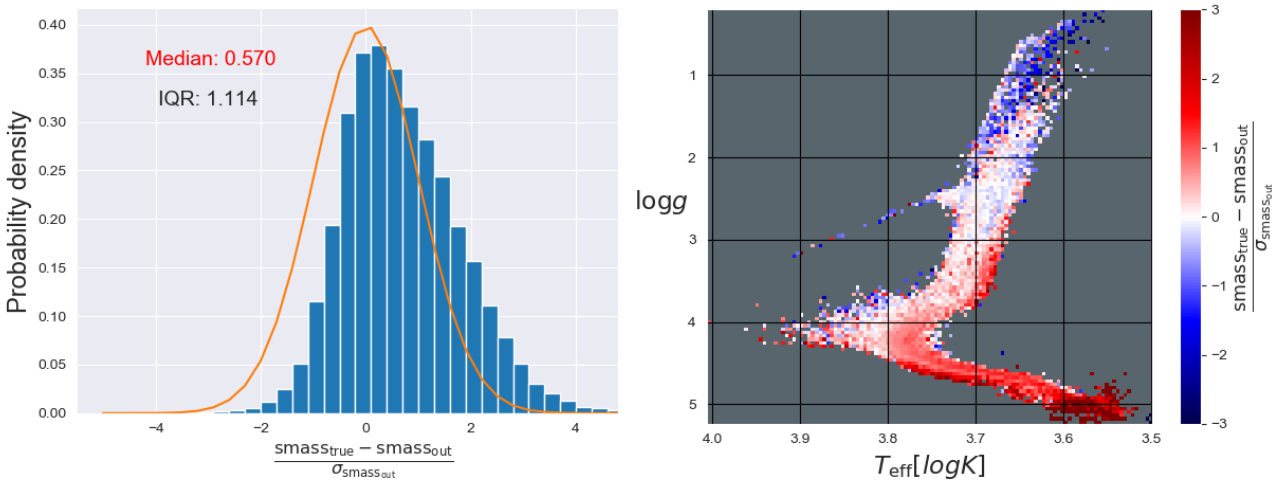

Figure 3.19: Comparison between true and calculated values for the masses of the virtual stars for the Kroupa IMF, using the Metallicity prior. On the left we see that the spread of the distribution has improved moderately compared to the previous cases, with only a slight increase in the median value. On the right we see that the giant branch is no longer mostly overestimated in mass (compared to fig. 3.4) which suggests that the Metallicity prior has helped. The underestimation problem in the main-sequence branch still remains however.

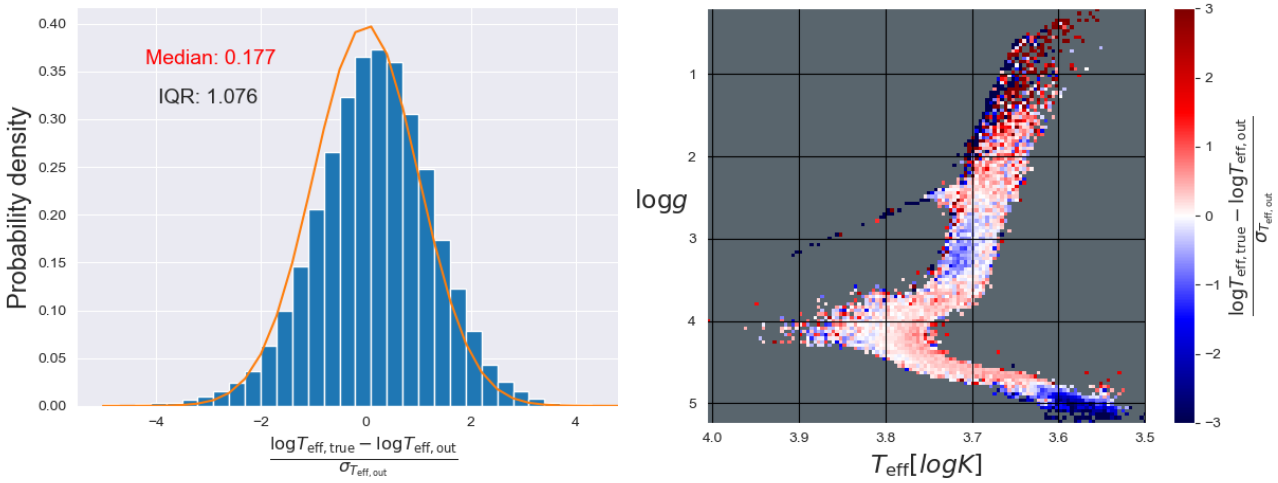

Figure 3.20: Comparison between true and calculated values for the effective temperatures of the virtual stars for the Kroupa IMF, using the Metallicity prior. Overall very little changes in both the distribution on the left and the plane on the right.

3.3.2 Chabrier IMF

Once again, almost no differences between the different IMFs. Overall better accuracy than the other two priors.

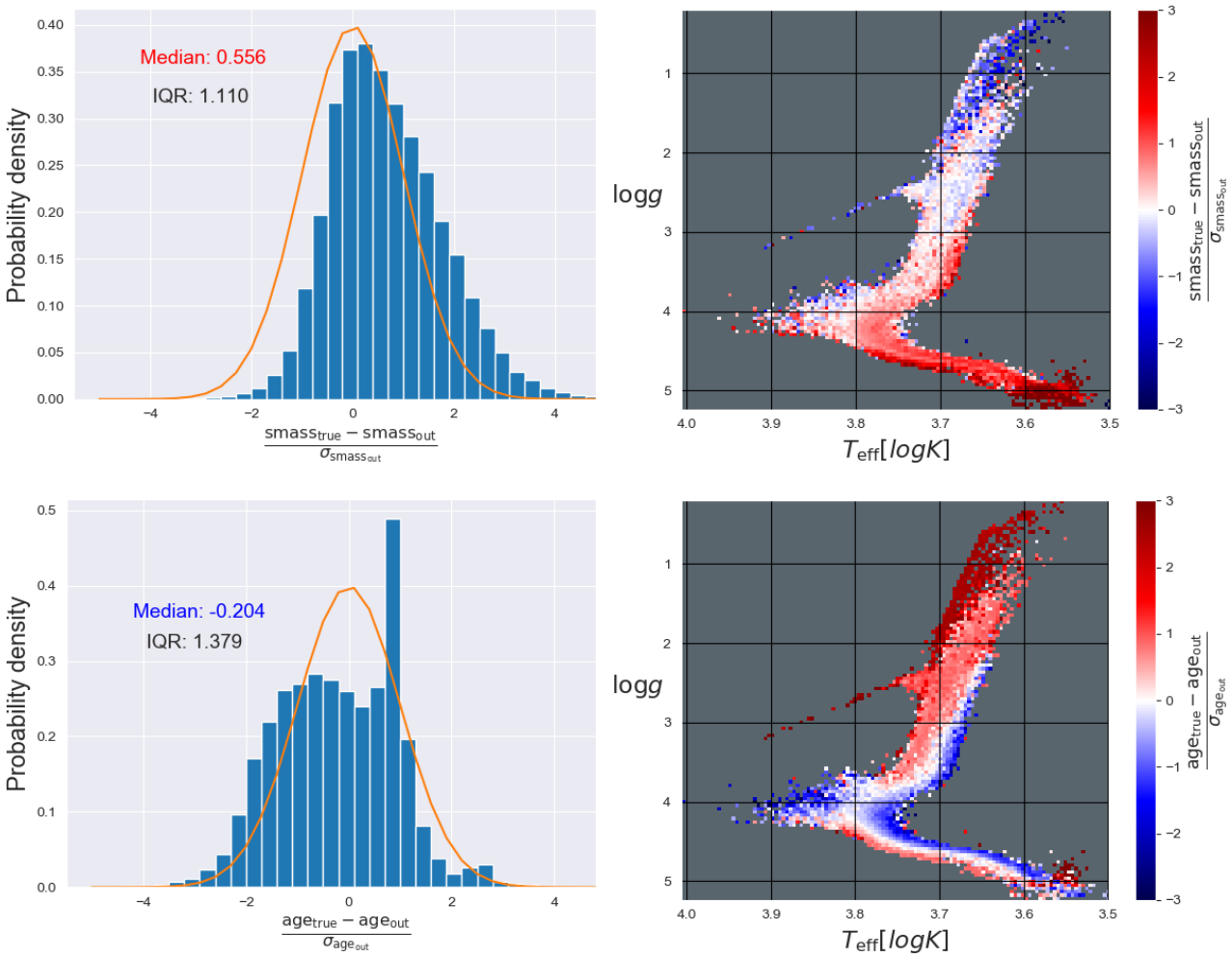

Figure 3.21: *Top:* Comparison between true and calculated values for the masses of the virtual stars for the Chabrier IMF, using the Metallicity prior. Once again, virtually no difference when compared to the Kroupa IMF. *Bottom:* Comparison between true and calculated values for the ages of the virtual stars for the Chabrier IMF, using the Metallicity prior. We see that on the left, the peculiar peak at 1 standard deviation still persists. Otherwise there are no major differences when compared to the Kroupa IMF.

3.3.3 Galaxia IMF

Similar to the other two IMFs, overall less spread out than the other two priors (albeit with slightly larger in magnitude median values).

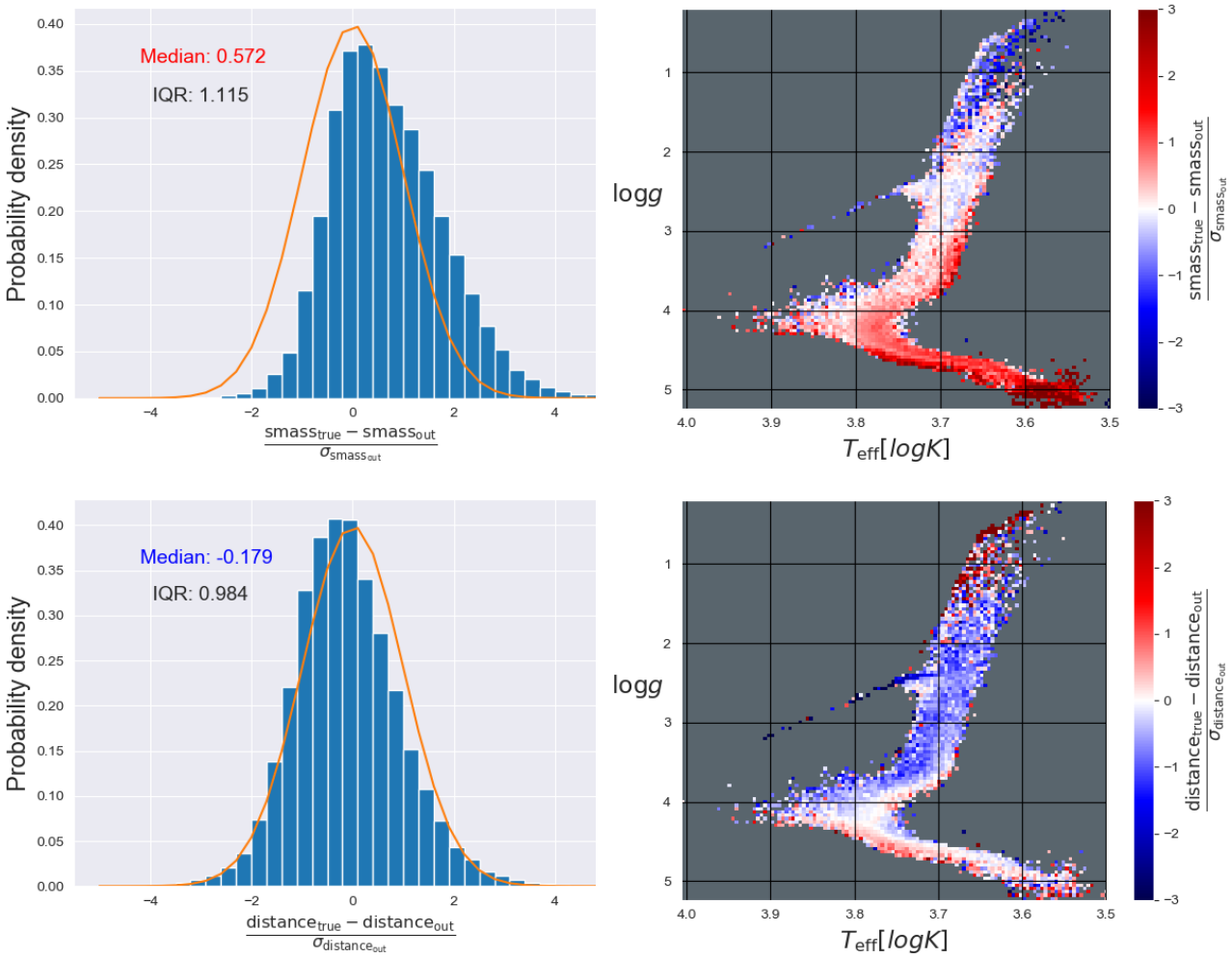

Figure 3.22: *Top:* Comparison between true and calculated values for the masses of the virtual stars for the Galaxia IMF, using the Metallicity prior. Almost no difference when compared to the previous IMFs. *Bottom:* Comparison between true and calculated values for the ages of the virtual stars for the Chabrier IMF, using the Metallicity prior. We see that on the left, the peculiar peak at 1 standard deviation still persists. Otherwise there are no major differences when compared to the other two IMFs.

3.4 Decreased parallax uncertainty

Finally we look at what happens when we use a smaller parallax uncertainty. Gaia DR2 (Luri et al. 2018) has typical ϖ uncertainties of 0.05 mas for these stars. We only use the Kroupa IMF since from previous sections it has been seen that the IMF does not seem to affect the results at all. We also try all 3 priors to see if it has any effect on the results (only illustrating the age and mass values for the Age and Metallicity priors for reasons which will become apparent).

For the age comparison, the results are mostly the same as for the previous measurements and the respective priors used (e.g. fig. 3.23). However the measurements for the other parameters are extremely unexpected (e.g. fig. 3.24). They do not make much sense since there are no immediately observable patterns to the apparent chaotic values. Surprisingly, the other least affected parameter seems to be the stellar mass (figures 3.26, 3.28, and 3.29) albeit still having an extremely large dispersion value.

It is not clear whether something went wrong with BDASP, the code used to analyse the data or if there are some underlying problems with decreasing the parallax uncertainty. In theory, the smaller uncertainty in the parallax should have improved the results. However that was not the case due to some unknown reason. The code has been checked many times and everything seemed to be in working order. There might also be a fundamental flaw in the approach itself. Thus, the results should be treated with caution.

3.4.1 Density prior

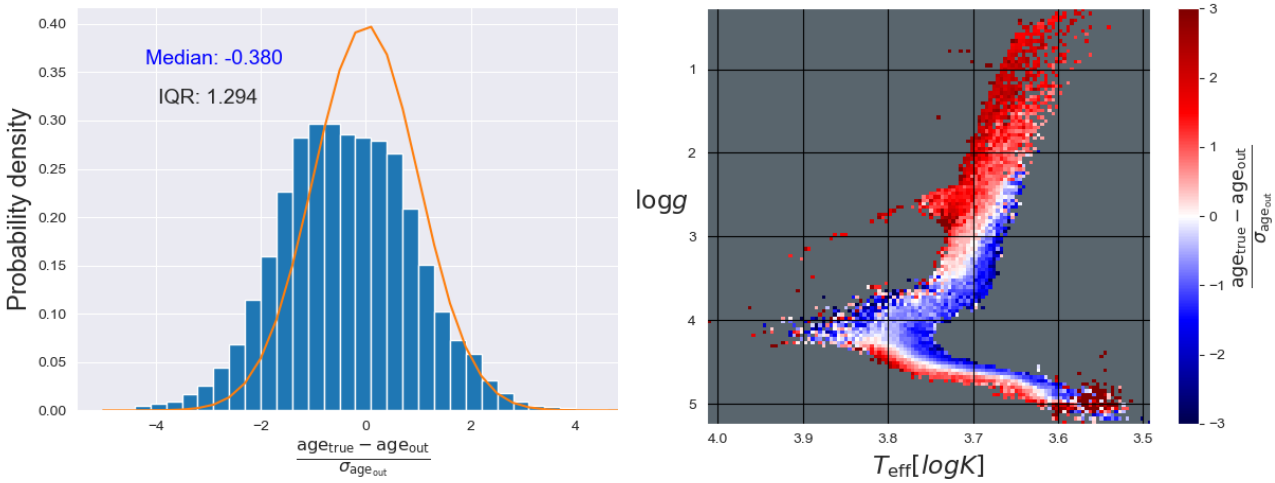

Figure 3.23: Comparison between true and calculated values for the age of the virtual stars for the Kroupa IMF, using the Density prior and reduced parallax uncertainty. The results seem similar to previous cases, albeit with a slightly larger dispersion and more underestimation.

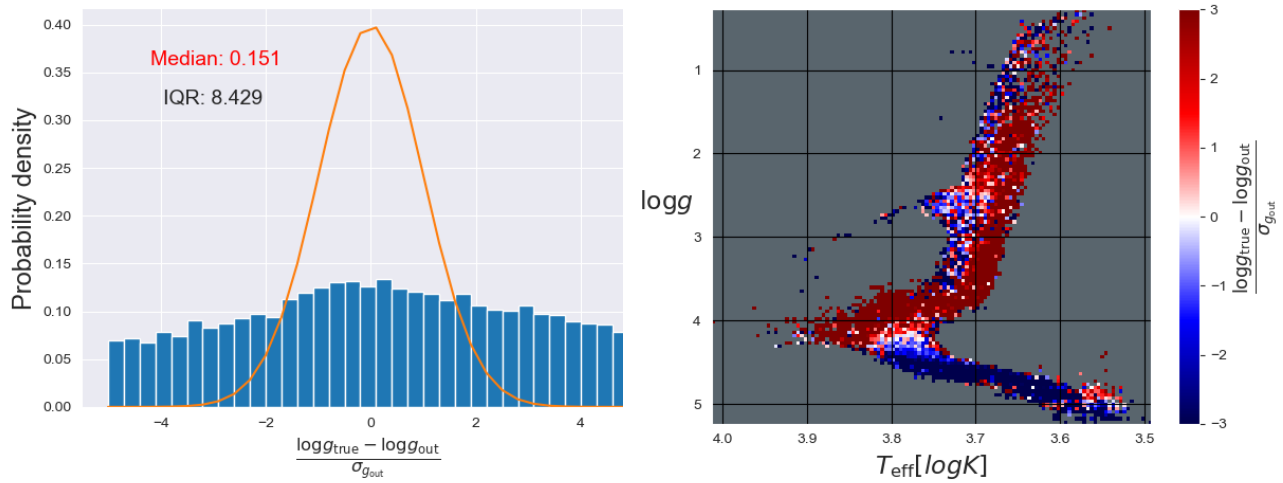

Figure 3.24: Comparison between true and calculated values for the surface gravity of the virtual stars for the Kroupa IMF, using the Density prior and reduced parallax uncertainty. It seems that the main-sequence stars are severely overestimated, while the opposite is true for the giants.

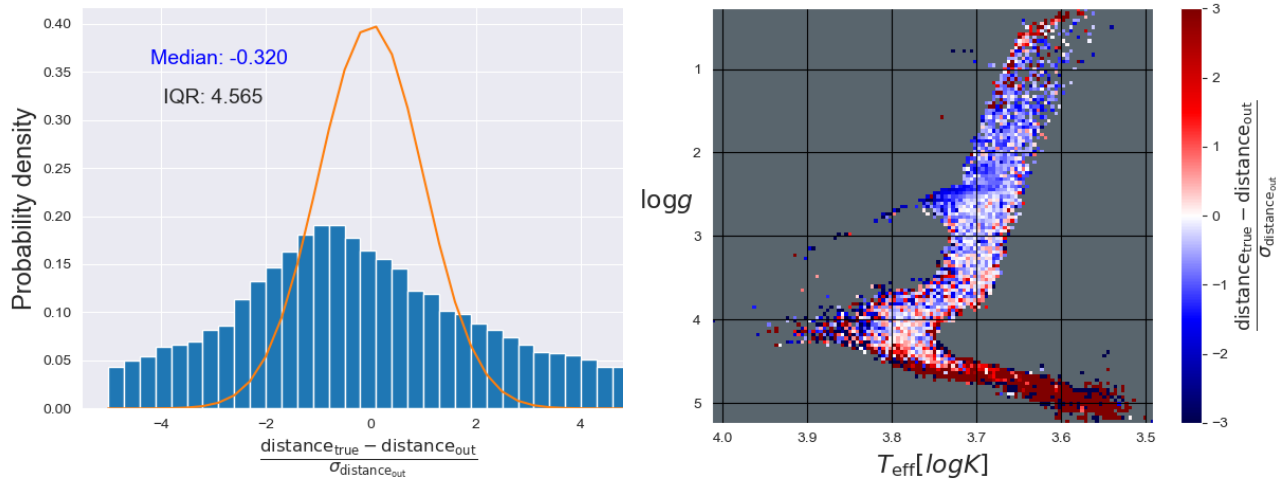

Figure 3.25: Comparison between true and calculated values for the distances of the virtual stars for the Kroupa IMF, using the Density prior and reduced parallax uncertainty. An overall overestimation for the giants can be seen, while the main-sequence stars are severely underestimated.

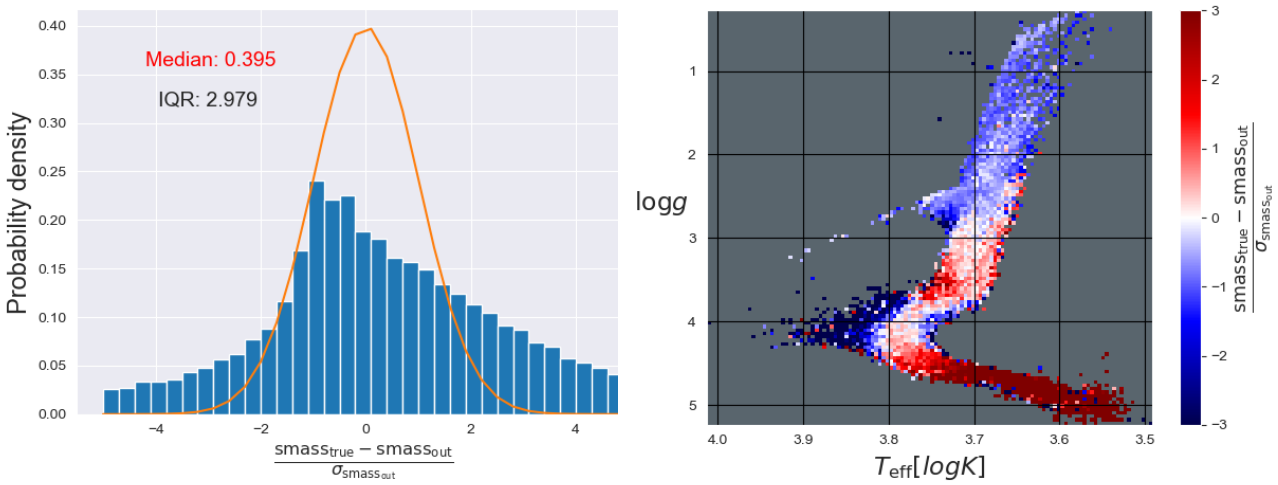

Figure 3.26: Comparison between true and calculated values for the masses of the virtual stars for the Kroupa IMF, using the Density prior and reduced parallax uncertainty. Surprisingly, most of the features in the right image persist from previous cases, although the spread is extremely large.

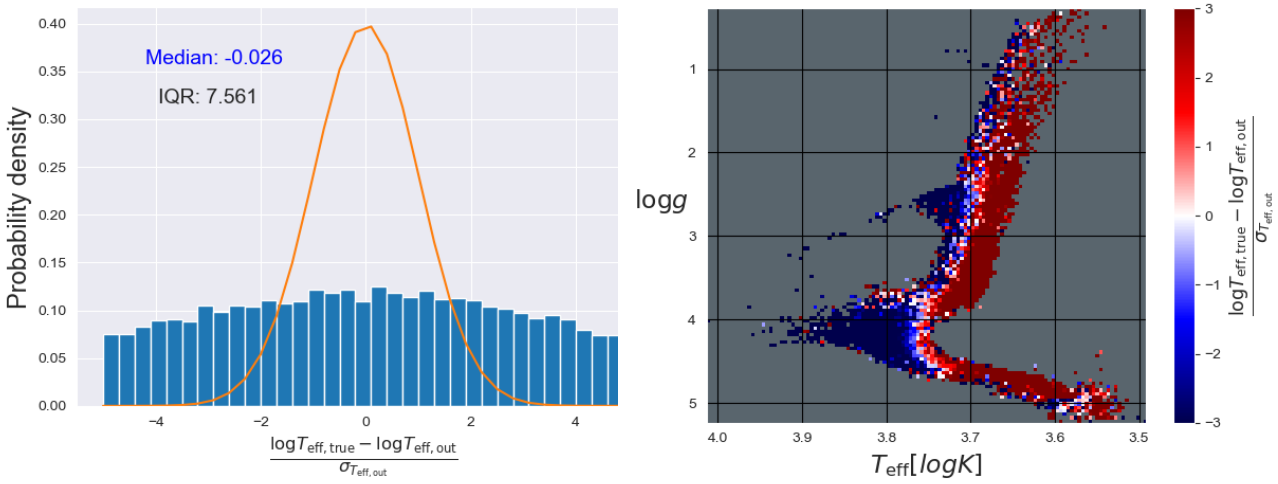

Figure 3.27: Comparison between true and calculated values for the effective temperatures of the virtual stars for the Kroupa IMF, using the Density prior and reduced parallax uncertainty. Seemingly a pattern which divides the plane in the right image takes shape. Early main-sequence stars and most of the giants seem to be severely underestimated, while the opposite is true for the rest of the zones.

3.4.2 Age prior

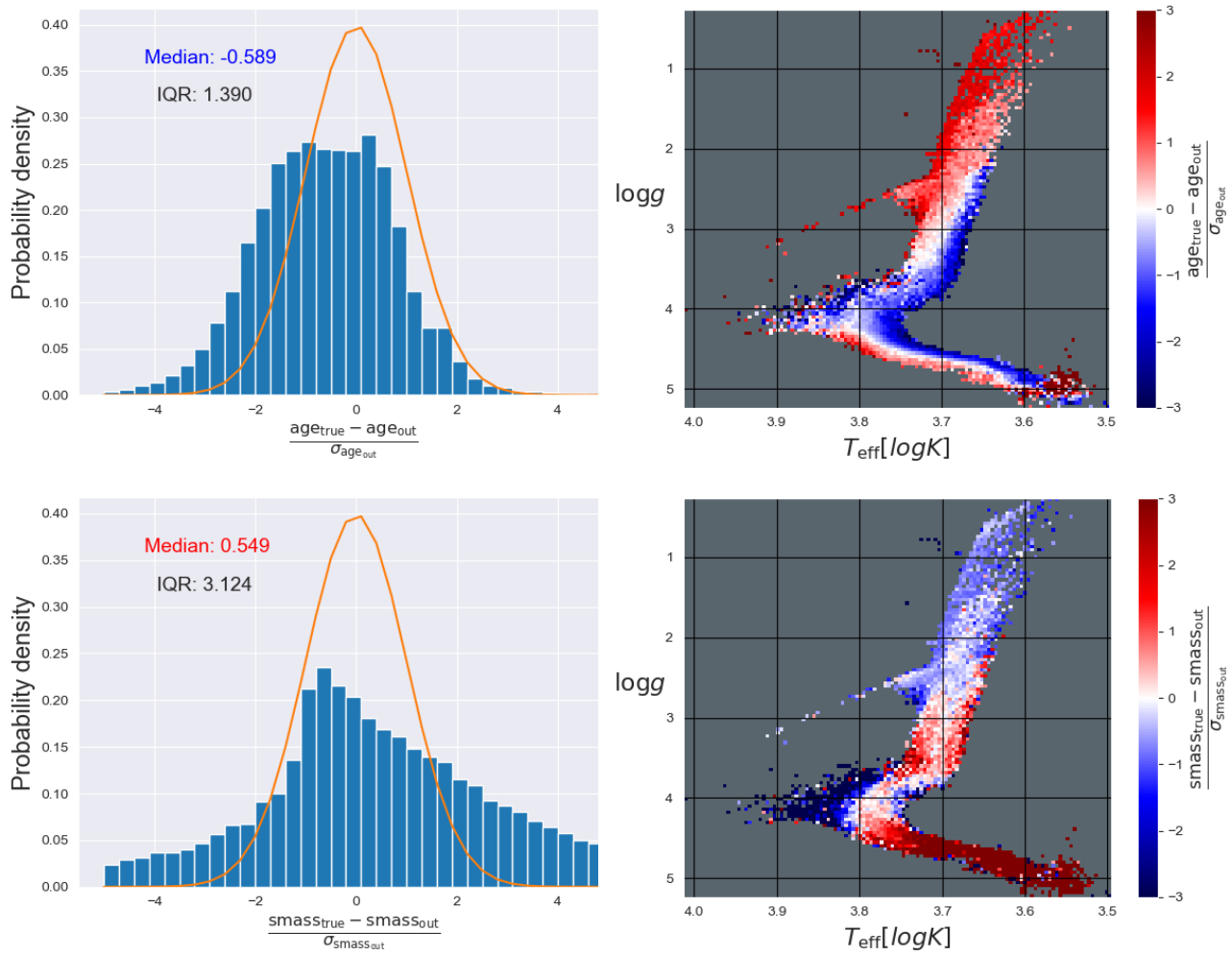

Figure 3.28: *Top:* Comparison between true and calculated values for the ages of the virtual stars for the Kroupa IMF, using the Age prior and reduced parallax uncertainty. Overall no immediately observable differences between this and the previous cases for larger parallax uncertainty (other than a slight increase in overestimation and spread). *Bottom:* Comparison between true and calculated values for the masses of the virtual stars for the Kroupa IMF, using the Age prior and reduced parallax uncertainty. Almost no difference compared to the previous case (fig. 3.26).

3.4.3 Metallicity prior

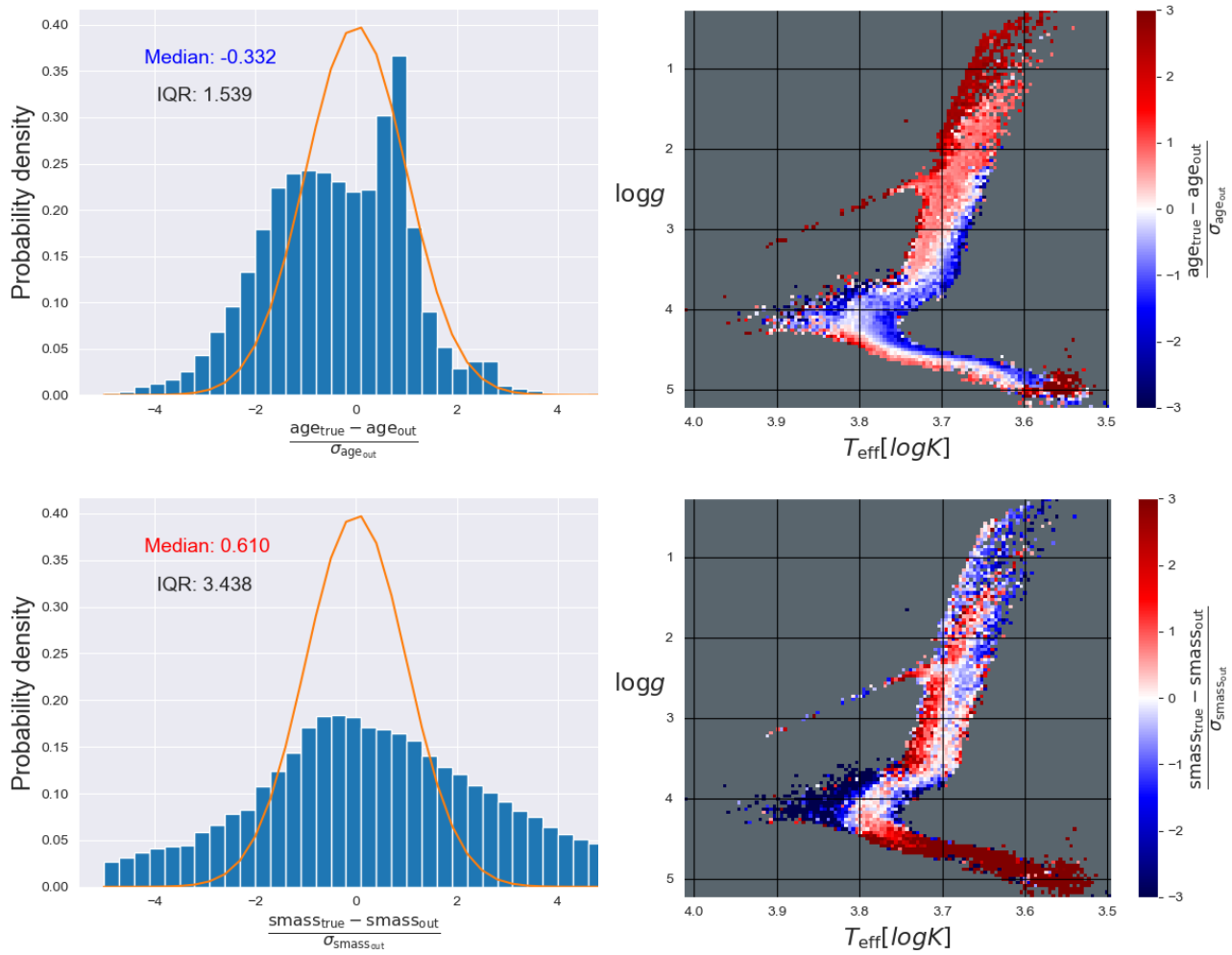

Figure 3.29: *Top:* Comparison between true and calculated values for the ages of the virtual stars for the Kroupa IMF, using the Age prior and reduced parallax uncertainty. We again observe the peculiar peak around 1 standard deviation. Otherwise no major differences between priors (other than the change in gradients which is consistent with the Metallicity prior). *Bottom:* Comparison between true and calculated values for the masses of the virtual stars for the Kroupa IMF, using the Age prior and reduced parallax uncertainty. Some minor differences in the gradients on the right figure can be observed. This is consistent with the changes that the Metallicity prior brought in previous cases.

Chapter 4

Conclusions & Outlook

As can be seen from the results obtained during this project and presented in chapter 3 there seems to be a non-negligible disagreement between the true and calculated values of stellar parameters. There is an offset which strongly depends on the position in the $\log g/T_{\text{eff}}$ plane. This is indeed an issue, as the latest projects and missions in Astronomy are relying on the same techniques in measuring and analysing real data. Therefore one should start looking for potential causes as soon as possible in order to correct previous data and prevent inaccuracies in future projects.

One possible culprit could be that there are differences between the isochrones used by Galaxia and those used by BDASP. Galaxia uses an older version of isochrones (Marigo et al. 2008 and older) while BDASP uses the PARSEC v1.1 set (Bressan et al. 2012). This could have introduced the systematic errors and differences in spread that we see in most of the data. The average uncertainties (provided by RAVE DR5, Kunder et al. 2017) could have also been the product of isochrones which differ from the ones used in our work.

Another cause could be related to the software used in this project. The Galaxia model priors and the ones used by BDASP are different. One difference mentioned in the results is that Galaxia makes use of the age-metallicity relation while BDASP does not. Other such differences could probably lead to unexpected results. However this would imply that the method used here is not robust against these differences. This definitely would constitute a big problem and would need further examination.

It may also be the case that for this complicated comparison, the Bayesian framework simply cannot produce unbiased results. There might be many more factors that come into play for the priors that we use to account for. Therefore other ways of treating this particular problem might yield better results.

Another approach could be to create a simpler model initially, which would behave as expected and give the true values with little to no error. Then, more layers of complexity (in the form of priors used in this project) can be added gradually. This way we could tell which step of this process would introduce the large differences we have seen, or the strange behaviour when it comes to decreasing the uncertainty (as seen for the parallax case, section 3.4).

Nevertheless, BDASP and Galaxia are not perfect, and thus it cannot be said for certain that there is indeed a problem to such a worrying extent. Perhaps, despite the author's best efforts, mistakes were made in the code used to analyse the data. Regardless, the author strongly encourages further studies to be done on this subject, possibly with better techniques that might uncover nuances which might have been brushed over in this project. Perhaps the available software needed to perform these tasks will have improved over time. Therefore, it would be in our interest to make sure we perform such checks on our techniques from time to time, so that we do not lose accuracy when trying to understand the stars that make up the Milky Way, and, by extension, other galaxies which make up the universe.

Acknowledgements

The author is grateful to Paul McMillan for his guidance during the whole project, offering ideas to try out and suggestions which helped improve the obtained results and this paper. The author is also grateful to the examiners of this paper, David Hobbs and Daohai Li, for offering suggestions which helped to improve the paper and might provide some leads to follow in future projects. The author would also like to thank Martin Montelius for translating the popular description of this project into Swedish. This work has made use of the Galaxia project (`http://galaxia.sourceforge.net/`), the RAVE project (`https://www.rave-survey.org/project/`), and Gaia DR2 (`https://www.cosmos.esa.int/web/gaia/dr2`).

Bibliography

Aumer, M. & Binney, J. J. 2009, Monthly Notices of the Royal Astronomical Society, 397, 1286

Box, G. E. P. & Tiao, G. C. 2011, Bayesian Inference in Statistical Analysis (Hoboken: John Wiley & Sons), description based upon print version of record.

Bressan, A., Marigo, P., Girardi, L., et al. 2012, MNRAS, 427, 127

Bullock, J. S. & Johnston, K. V. 2005, ApJ, 635, 931

Kroupa, P. 2001, Monthly Notices of the Royal Astronomical Society, 322, 231

Kunder, A., Kordopatis, G., Steinmetz, M., et al. 2017, AJ, 153, 75

Luri, X., Brown, A. G. A., Sarro, L. M., et al. 2018, A&A, 616, A9

Marigo, P., Girardi, L., Bressan, A., et al. 2008, A&A, 482, 883

McMillan, P. J., Kordopatis, G., Kunder, A., et al. 2018, MNRAS, 477, 5279

Rieke, G. H. & Lebofsky, M. J. 1985, ApJ, 288, 618

Robin, A. C., Reylé, C., Derrière, S., & Picaud, S. 2003, A&A, 409, 523

Romano, D., Chiappini, C., Matteucci, F., & Tosi, M. 2005, A&A, 430, 491

Schlegel, D. J., Finkbeiner, D. P., & Davis, M. 1998, ApJ, 500, 525

Sharma, S., Bland-Hawthorn, J., Johnston, K. V., & Binney, J. 2011, ApJ, 730, 3

Sourceforge. 2011, Galaxia Code Instructions, `http://galaxia.sourceforge.net/Galaxia3pub.html`, [Online; accessed 29-03-2019]

Appendix A

Parameters & equations

Table A.1: Table containing the most relevant parameters used by Galaxia when generating a survey. Information taken from the Galaxia code instructions (Sourceforge 2011).

Parameter	Description
photoSys	Photometric system used (in our surveys we used DCMC, which contains the I, J, H, K_s filters.)
magColorNames	i.e. J, J-K_s (first one will be affected by the apparent magnitude limits, second one will be affected by the colour limits)
appMagLimits[0], appMagLimits[1]	Lower and upper apparent magnitude limits (for our surveys, from 9 to 12)
geometryOption	0 for the whole sky or 1 for a circular patch (the latter being the one we used)
longitude, latitude, surveyArea	Parameters used when working with a circular patch for galactic longitude and latidude, and the area covered by the patch (e.g.: 90°, 0°, 100 $^{\circ 2}$)
fSample	The fraction of stars generated in the survey (1.0 for the whole correct number of stars, or lower for subsampling)
seed	Numerical sequence of numbers used to generate random numbers (e.g.: 54)

Table A.2: Table containing the parameters given as input to BDASP, in the form of stellar observables.

Name	Notation
Effective temperature	T_{eff}
Surface gravity (logarithmic)	$\log g$
Metallicity	[M/H]
Apparent magnitudes in near-infrared bands	J, H, K_s
Parallax	ϖ

Table A.3: Table containing the parameters modeled by BDASP (and given as output), in the form of stellar observables.

Name	Notation
Mass	$\mathcal{M}$
Age	$\log g$
Metallicity	[M/H]
Galactic coordinates	l, b
Distance	s
Extinction in V-band	A_V

Table A.4: Geometry of stellar components. The formulas used are from Robin et al. 2003. Note, (R, θ, z) are the coordinates in the galactocentric cylindrical coordinate system and $a^2 = R^2 + \frac{z - z_{\rm warp}}{{\rm k_{flare}}\epsilon(\tau)}$ (for the thin disc).

Component	Age (Gyr)	density law $\rho(\mathbf{r}, \tau)$
Thin Disc	≤ 0.15	$\frac{\rho_c \Psi(\tau)}{k_{\rm flare}\epsilon(\tau)}\{\exp(-(a/h_{R+})^2) - \exp(-(a/h_{R-})^2)\}$
		where: $h_{R+} = 5000$ pc, $h_{R-} = 3000$ pc
		IMF- $\xi(m) \propto m^{-1.6}$ for $m < 1\ M_\odot$ and $\xi(m) \propto m^{-3.0}$ for $m > 1\ M_\odot$
Thin Disc	0.15–10	$\frac{\rho_c \Psi(\tau)}{k_{\rm flare}\epsilon(\tau)}\{\exp(-(0.5^2 + \frac{a^2}{h_{R+}^2})) - \exp(-(0.5^2 + \frac{a^2}{h_{R-}^2}))\}$
		where: $h_{R+} = 2530$ pc, $h_{R-} = 1320$ pc,
		IMF- $\xi(m) \propto m^{-1.6}$ for $m < 1\ M_\odot$ and $\xi(m) \propto m^{-3.0}$ for $m > 1\ M_\odot$
Thick disc	11	if $\lvert z\rvert \leq x_l$, $\rho_c \delta(\tau - 11) \exp\left(-\frac{R - R_\odot}{h_R}\right) \times \left(1 - \frac{1/h_z}{x_l \times (2. + x_l/h_z)} \times z^2\right)$
		if $\lvert z\rvert > x_l$, $\rho_c \delta(\tau - 11) \exp\left(-\frac{R - R_\odot}{h_R}\right) \times \frac{\exp(x_l/h_z)}{1 + x_l/2h_z} \exp(-\frac{\lvert z\rvert}{h_z})$
		where: $h_R = 2500$ pc, $h_z = 800$ pc, $x_l = 400$ pc
		IMF- $\xi(m) \propto m^{-0.5}$
Spheroid	14	$\rho_c \delta(\tau - 14) \left(\frac{{\rm Max}(a_{\rm c}, a)}{R_\odot}\right)^{n_{\rm H}}$
		where: $a^2 = R^2 + \frac{z^2}{\epsilon^2}$,
		$a_{\rm c} = 500$ pc, $\epsilon = 0.64$, $n_{\rm H} = -2.77$
		IMF- $\xi(m) \propto m^{-0.5}$
Bulge	10	if $\sqrt{x^2 + y^2} < R_{\rm c}$, $\rho_c \delta(\tau - 10) \exp(-0.5 r_{\rm s}^2)$
		if $\sqrt{x^2 + y^2} > R_{\rm c}$, $\rho_c \delta(\tau - 10) \exp(-0.5 r_{\rm s}^2) \times \exp(-0.5(\frac{\sqrt{x^2 + y^2} - R_{\rm c}}{0.5})^2)$
		where: $r_s^2 = \sqrt{[(\frac{x}{x_0})^2 + (\frac{y}{y_0})^2]^2 + (\frac{z}{z_0})^4}$,
		$R_{\rm c} = 2.54$, $x_0 = 1.59$, $y_0 = z_0 = 0.424$, $\alpha = 78.9°$, $\beta = 3.5°$, $\gamma = 91.3°$
		IMF- $\xi(m) \propto m^{-2.35}$
ISM		$\rho_c \exp(-\frac{R - R_\odot}{h_R}) \times \exp(-\frac{\lvert z\rvert}{h_z})$
		where: $h_R = 4500$ pc, $h_z = 140$ pc
Dark halo		$\frac{\rho_{\rm c}}{(1. + (a/R_{\rm c})^2)}$
		where: $R_{\rm c} = 2697$ pc and $\rho_{\rm c} = 0.1079$